Proceedings of the CAS-CERN Accelerator School: Intensity Limitations in Particle Beams, Geneva, Switzerland, 2–11 November 2015, edited by W. Herr, CERN Yellow Reports: School Proceedings, Vol. 3/2017, CERN-2017-006-SP (CERN, Geneva, 2017)

# Space Charge in Circular Machines

*G. Franchetti*
GSI Helmholtzzentrum für Schwerionenforschung, Darmstadt, Germany

**Abstract**
Direct Coulomb forces play an important role in beam transport and storage. In this paper, the effect of space charge in beams stored in circular machines is reviewed. Starting from the concept of a matched beam, the most common particle distributions are introduced. Space charge forces are first addressed as 'external frozen' forces and, in this approximation, the modification of the machine optics is discussed, as well as the matching of high-intensity beams. Envelope equations and r.m.s. equivalence are presented as relevant tools for matching high-intensity beams. The space charge limit, space charge tune-shift, tune-spread and their relation with resonances are covered. The more general beam response to Coulomb forces is discussed for mismatched beams, and a derivation of the coherent frequencies is presented for a Kapchinsky–Vladimirsky beam. The concept of free energy is examined in detail, as a source of emittance increase for high-intensity beams. More complex and relevant examples are presented with the fully coupled envelope equations, and the interplay of coherent and incoherent effects is addressed in the Montague resonance. Space charge as driving incoherent resonances is discussed. Longitudinal dynamics in the presence of space charge are briefly presented as well.

**Keywords**
CERN report; space charge.

## 1 Introduction

In the following, we will discuss the effect of space charge in circular machines. We will first focus on describing the dynamics of a single particle within a beam. For coasting beams, we use a reference frame co-moving with the reference particle; hence, the co-ordinates $x, y$ used to identify the positions of a particle are meant with respect to the design orbit. Para-axial approximation is used and, as usual, $x' = \mathrm{d}x/\mathrm{d}s, y' = \mathrm{d}y/\mathrm{d}s$, where $s$ is the longitudinal co-ordinate set on the reference orbit.

## 2 Matched beams at low intensity

We consider in our discussion a beam distribution for two-dimensional (2D) beams, i.e., a coasting beam. Typically, a 2D beam is characterized by a constant charge-line density of $\lambda = \mathrm{d}q/\mathrm{d}s$, and its most general transverse particle density at longitudinal position $s$ is defined as

$$\rho(x,x',y,y',s) = \frac{\mathrm{d}q}{\mathrm{d}x\mathrm{d}x'\mathrm{d}y\mathrm{d}y'\mathrm{d}s} = \lambda n(x,x',y,y',s)\,.$$

The form of the normalized function $n(x,x',y,y',s)$ allows a complete characterization of the transverse beam distribution. The normalization condition on $n(x,x',y,y',s)$ is obtained by the requirement

$$\int n(x,x',y,y',s)\mathrm{d}x\mathrm{d}x'\mathrm{d}y\mathrm{d}y' = 1\,. \tag{1}$$

The variable $s$ in $n()$ says that the beam distribution may change along the machine; this aspect will be discussed later.



https://doi.org/10.23730/CYRSP-2017-003.353

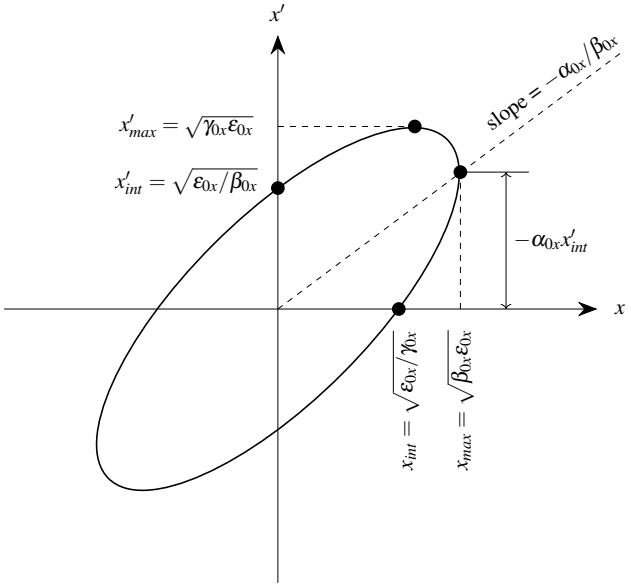


**Fig. 1:** Courant–Snyder ellipse: $\varepsilon_{0x}$, single-particle emittance; area $= \pi\varepsilon_{0x}$

In a circular accelerator, the transverse dynamical properties of a low-intensity beam at an arbitrary longitudinal position $s$ is determined by the Poincaré section, which for a linear motion is completely described by the Courant–Snyder theory [1]. We will consider 2D beams matched with the optics. A matched beam means that the transverse beam distribution at the section $s$ will be the same after the beam has travelled for one machine turn. In this sense, the property of a particle beam to be matched is related with the Courant–Snyder ellipses, shown in Fig. 1. In the absence of coupling, the planes $x$–$x'$ and $y$–$y'$ can be treated independently. At the longitudinal position $s$ in the plane $x$–$x'$, turn after turn, a particle performs jumps, remaining on a distinct ellipse. Each jump corresponds to a phase jump of $2\pi Q_{0x}$, with $Q_{0x}$ the horizontal machine tune. Similar dynamics happen in the vertical plane. If only one particle is considered, clearly we can distinguish where it is turn after turn. Therefore, in the sense previously defined, a single particle cannot be 'matched' with the machine optics. However, if an ellipse is 'uniformly' populated by particles, then after one turn there is no way for an observer sitting at position $s$ to tell that the beam has made one turn around the machine.

A beam uniformly filling 'one' Courant–Snyder ellipse is then matched. More generally, we can think of a matched beam as a collection of uniformly filled Courant–Snyder ellipses, each with an arbitrary particle density. This means that the most general matched beam distribution is a function of the Courant–Snyder invariants; hence, the normalized function $n()$ is written as

$$n(\varepsilon_{0x}, \varepsilon_{0y}, s)\,. \tag{2}$$

In this formula, the $s$ dependence simply means that the function $n()$ may change along the machine. This mathematical formula (Eq. (2)) says that the particle density depends on the value of the quantities $\varepsilon_{x0}, \varepsilon_{y0}$, which are defined by the expressions:

$$\begin{aligned} \varepsilon_{0x} &= \gamma_{0x}x^2 + 2\alpha_{0x}xx' + \beta_{0x}x'^2\,, \\ \varepsilon_{0y} &= \gamma_{0y}y^2 + 2\alpha_{0y}yy' + \beta_{0y}y'^2\,. \end{aligned} \tag{3}$$

The optical functions

$$\gamma_{0x}, \alpha_{0x}, \beta_{0x}, \gamma_{0y}, \alpha_{0y}, \beta_{0y}\,, \tag{4}$$

are here computed at the longitudinal position $s$ where the Poincaré section is studied. The function $n()$ in Eq. (2) yields the same value when the co-ordinates $x,x',y,y'$ keep $\varepsilon_{0x},\varepsilon_{0y}$ unchanged; therefore, this means that a distribution modelled with a normalized function like Eq. (2), i.e., depending on $\varepsilon_{0x},\varepsilon_{0y}$, will produce a particle distribution matched with the optics at section $s$ because all the Courant–Snyder ellipses are uniformly populated. The index 0 in the optical functions (Eq. (4)) is used to indicate that $\varepsilon_{0x}$ and $\varepsilon_{0y}$ are computed for weak space charge, virtually absent.

The function of Eq. (2) yields the most general expression for a matched distribution. However, some other consideration has to be used to model beam distributions more realistically: an energy conservation is here invoked, which basically 'incorporates' the physics of the source, all optics manipulations of linacs, and schemes of injection in the ring. As a consequence, a correlation is assumed in the single-particle energy between both planes, and the general matched particle distribution can be written as

$$n(x,x',y,y',s) = \frac{1}{\pi^2 \mathscr{E}_x \mathscr{E}_y} \tilde{n}\left(\frac{\varepsilon_{0x}(x,x')}{\mathscr{E}_x} + \frac{\varepsilon_{0y}(y,y')}{\mathscr{E}_y}\right), \tag{5}$$

where $\mathscr{E}_x$, and $\mathscr{E}_y$ are some 'scaling' factors, which define the geometrical extension of the distribution in the 4D phase space. In this expression, we drop the dependence of $s$ in $\tilde{n}()$ because, by our definition, the matched distribution must be periodic, and the periodicity is already included into the optic functions. The absence of $s$ in the function $\tilde{n}()$ also means that the type of distribution does not change and remains the same (at this point of the discussion, this is an ansatz). The normalization condition Eq. (1) applied to Eq. (5) reads

$$\int_0^\infty \tilde{n}(t) t \mathrm{d}t = 1\,.$$

with $\tilde{n}(t)$ defined in $0 \le t < \infty$.

## 3 Main types of beam distribution

According to the type of function $\tilde{n}$ we use, a different type of matched beam distribution is obtained. The mostly used beam distributions are as follows.

1. Kapchinsky–Vladimirsky:

$$n(x,x',y,y',s) = \frac{1}{\pi^2 \mathscr{E}_x \mathscr{E}_y} \delta\left(\frac{\varepsilon_{0x}}{\mathscr{E}_x} + \frac{\varepsilon_{0y}}{\mathscr{E}_y} - 1\right), \tag{6}$$

   where $\delta()$ is the Dirac delta function.

2. Waterbag:

$$n(x,x',y,y',s) = \frac{2}{\pi^2 \mathscr{E}_x \mathscr{E}_y} \Theta\left(1 - \frac{\varepsilon_{0x}}{\mathscr{E}_x} - \frac{\varepsilon_{0y}}{\mathscr{E}_y}\right), \tag{7}$$

   where $\Theta()$ is the Heaviside function.

3. Gaussian:

$$n(x,x',y,y',s) = \frac{1}{4\pi^2 \mathscr{E}_x \mathscr{E}_y} \mathrm{e}^{-\frac{1}{2}\left(\frac{\varepsilon_{0x}}{\mathscr{E}_x} + \frac{\varepsilon_{0y}}{\mathscr{E}_y}\right)}. \tag{8}$$

In all these distributions, it is understood that $\varepsilon_{0x},\varepsilon_{0x}$ are the functions in Eq. (3).

As the space charge forces are determined by the spatial particle distribution, it is convenient to discuss the general form of a 2D matched beam in the $x$–$y$ plane. This distribution is proportional to the projection of $n(x,x',y,y')$ on the $x$–$y$ space, which, for convenience, we call $n(x,y)$, and is readily obtained from

$$n(x,y,s) = \int n(x,x',y,y',s)\mathrm{d}x'\mathrm{d}y'\,.$$

**Table 1:** Functions $\tilde{n}(t)$, and $\hat{n}(t)$ for the beam distribution discussed.

| | Kapchinsky–Vladimirsky | Waterbag | Gaussian |
|---|---|---|---|
| $\tilde{n}(t)$ | $\delta(t-1)$ | $2\Theta(1-t)$ | $\frac{1}{4}e^{-t/2}$ |
| $\hat{n}(t)$ | $\Theta(1-t)$ | $2(1-t)\Theta(1-t)$ | $\frac{1}{2}e^{-t/2}$ |

A direct integration of this equation using $n(x,x',y,y',s)$ given by Eq. (5) yields

$$n(x,y,s) = \frac{1}{\pi a_0(s) b_0(s)} \left[ F(\infty) - F\left( \frac{x^2}{a_0^2(s)} + \frac{y^2}{b_0^2(s)} \right) \right], \tag{9}$$

where $F(t) = \int_0^t \tilde{n}(t')\mathrm{d}t'$ is the primitive of $\tilde{n}(t)$. We also define $a_0(s) = \sqrt{\beta_{0x}(s)\mathscr{E}_x}$ and $b_0(s) = \sqrt{\beta_{0y}(s)\mathscr{E}_y}$. These quantities are related to the 'beam sizes' at the longitudinal positions $s$; in particular, for finite beam distribution, $a_0(s), b_0(s)$ are exactly the beam sizes. It is convenient to rewrite Eq. (9) in the form

$$n(x,y,s) = \frac{1}{\pi a_0(s) b_0(s)} \hat{n}\left( \frac{x^2}{a_0^2(s)} + \frac{y^2}{b_0^2(s)} \right), \tag{10}$$

with $\hat{n}(t) = F(\infty) - F(t)$ defined in $0 \le t < \infty$. From the property of $n(t)$ it follows that $\hat{n}(t)$ must satisfy the normalization condition $\int_0^\infty \hat{n}(t)\mathrm{d}t = 1$. Equation (10) is the most general expression of the normalized spatial 2D beam distribution for a matched beam. The Table 1 shows the functions $\tilde{n}(t)$, and $\hat{n}(t)$ for the main beam distributions.

To clarify the difference between the particle distributions in Eqs. (6)–(8), we plot each of them in several planes. Figure 2 shows the particle distribution in the $x$–$y$, $x$–$x'$, and $x$ profiles for the three types of distributions here discussed. The top row of the figures shows the properties of the Kapchinsky–Vladimirsky distribution. The two particle distributions in the $x$–$y$ and $x$–$x'$ profiles show a peculiar characteristic of the Kapchinsky–Vladimirsky distribution, namely that the projection in any plane yields constant particle density. This is a general property of the Kapchinsky–Vladimirsky distribution. The second row of figures refers to a waterbag distribution, and we see that the $x$–$y$ projection is more dense in the centre. This is also seen by a more pronounced peaked beam profile. The last row of figures shows the properties of a Gaussian distribution, truncated for convenience at $\varepsilon_{0x}/\mathscr{E}_x + \varepsilon_{0y}/\mathscr{E}_y \le 16$.

## 4 Space charge forces for a frozen distribution

For a static particle distribution in which each particle has position $\vec{r}_i$ and charge $q$, the electric field at the position $\vec{r}$ is given by Coulomb's law:

$$\vec{E}(\vec{r}) = \frac{q}{4\pi\varepsilon_0} \sum_i \frac{\vec{r} - \vec{r}_i}{|\vec{r} - \vec{r}_i|^3},$$

where $\varepsilon_0$ is the permittivity of vacuum.

Next, we analyse the electric field produced in coasting beams transported in alternating focusing structures. In this case, the electric field is computed with the approximation of a 'local coasting beam': the beam sizes $a_0(s), b_0(s)$ vary because of the optics, and their values change following some wavelength $\Delta s$, which depends on the particular optics; see Fig. 3 for an illustration with sizes altered for convenience. If $\Delta s \gg a_0, b_0$, then at the longitudinal position $s$, the transverse electric field is in good approximation, computed from the coasting beam with constant sizes that mimics the transverse particle distribution at $s$. In Fig. 3, this coasting beam with constant sizes is shown with black dashed lines. At the section $s$, the electric field of the actual 2D beam and that of the mimic beam are practically the same. In this approximation, the electric field on a transverse plane at the section $s$ is computed by the coasting beam

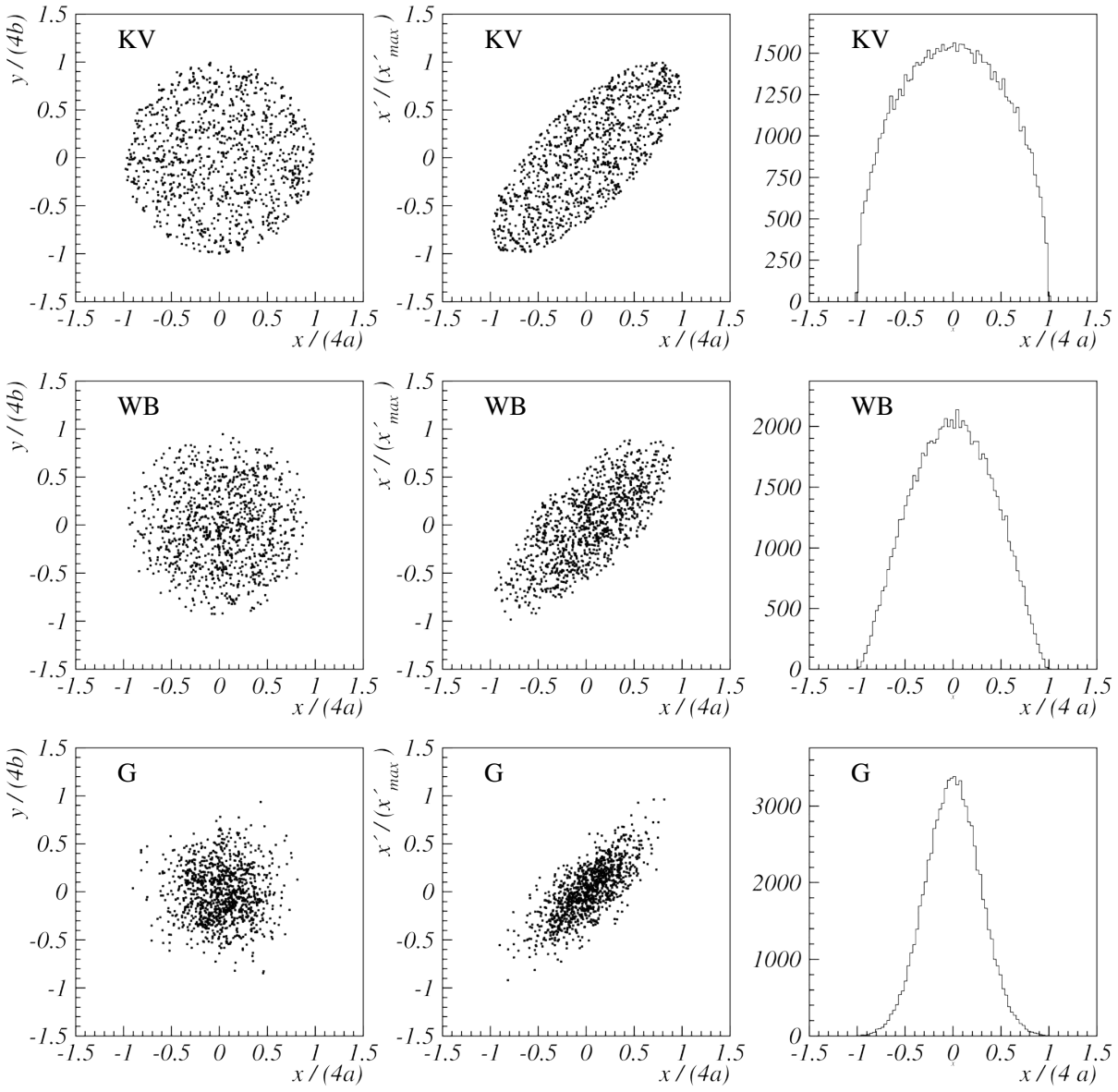


**Fig. 2:** Projections of (top) Kapchinsky–Vladimirsky (KV), (middle) waterbag (WB), and (bottom) Gaussian distributions. The right-hand column shows the change in the $x$ beam profile.

with the charge distribution $\rho(x,y,s) = \lambda n(x,y,s)$ (see Fig. 3). In the simple case of an axi-symmetric beam of radius $a_0 = b_0$ with a uniform beam density, the radial electric field $E_r(s)$ is given by

$$E_r(s) = \begin{cases} \frac{\rho(s)}{2\varepsilon_0} r & \text{if} \quad r \le a_0\,, \\ \frac{\rho(s) a_0^2(s)}{2\varepsilon_0} \frac{1}{r} & \text{if} \quad r \ge a_0\,. \end{cases} \tag{11}$$

The characteristic shape of this function is shown in Fig. 4. The next more complex situation is with an axi-symmetric non-uniform beam. The general expression of the electric field for an axi-symmetric beam distribution with density $\rho(r,s)$ is readily found by using Gauss's law

$$E_r(r,s) = \frac{1}{\varepsilon_0} \frac{1}{r} \int_0^r \rho(r',s) r' \mathrm{d}r'\,. \tag{12}$$

Note that this expression at section $s$ holds only if $a_0 = b_0$ in Eq. (9). This condition is equivalent to $\beta_{0x}\mathscr{E}_x = \beta_{0y}\mathscr{E}_y$ .

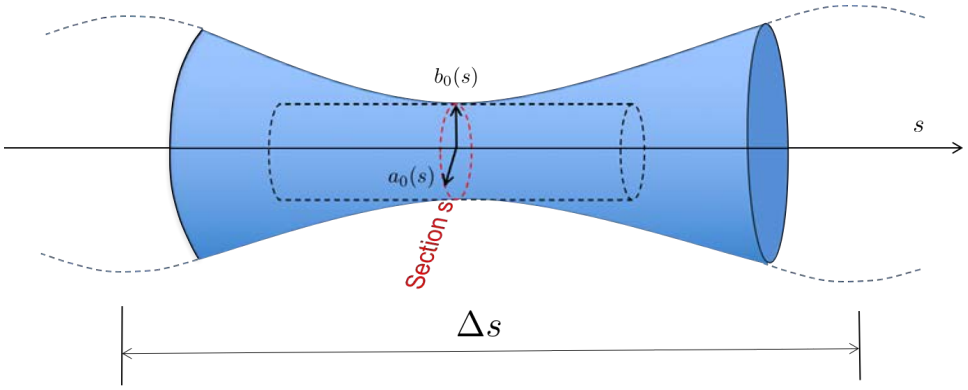


**Fig. 3:** Local coasting beam approximation

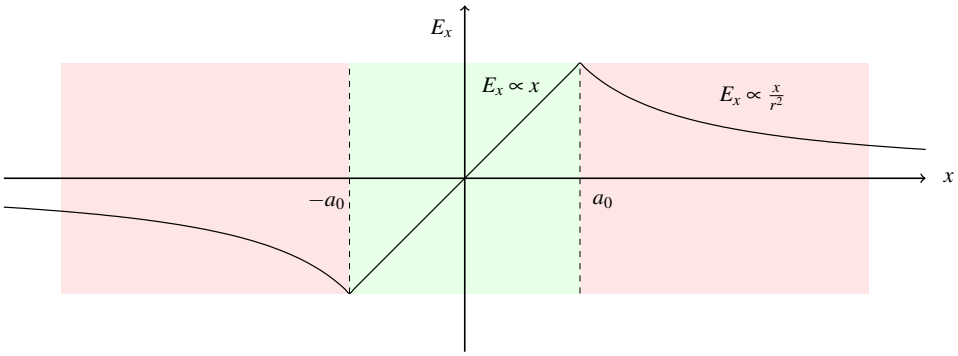


**Fig. 4:** Radial electric field in an axi-symmetrical beam

If at position $s$, we have $\beta_{0x}\mathscr{E}_x \neq \beta_{0y}\mathscr{E}_y$ i.e., $a_0 \neq b_0$, then Eq. (12) no longer holds. In this case, the computation of the electric field becomes more difficult, as it has to account for the different axis symmetry. The physical $x$–$y$ charge density of the beam is given by $\rho(x,y) = \lambda n(x,y)$ with $n(x,y)$ from Eq. (10). It is now convenient to define Eq. (10) as

$$n(x,y) = \frac{\hat{n}(T)}{\pi a_0 b_0}\,, \tag{13}$$

with $T$ an iso-density parameter

$$T = \frac{x^2}{a_0^2} + \frac{y^2}{b_0^2}\,.$$

With the use of these definitions, the transverse electric field is found by the integral

$$E_x = \frac{\lambda}{2\pi\varepsilon_0} x \int_0^\infty \frac{\hat{n}(\hat{T})}{(a_0^2+t)^{3/2}(b_0^2+t)^{1/2}}\mathrm{d}t\,, \tag{14}$$

where the variable $\hat{T}$ is defined as

$$\hat{T} = \frac{x^2}{a_0^2+t} + \frac{y^2}{b_0^2+t}\,. \tag{15}$$

The derivation of this expression is given in Ref. [2]. The electric field $E_y$ is obtained by exchanging $x \leftrightarrow y$ and $a_0 \leftrightarrow b_0$. It is straightforward to verify that Eq. (14) yields Eq. (12) for the case of $a_0 = b_0$; in fact, in this case we obtain

$$E_x = \frac{\lambda}{2\pi\varepsilon_0} x \int_0^\infty \frac{\hat{n}\left(\frac{r^2}{a_0^2+t}\right)}{(a_0^2+t)^2}\mathrm{d}t \tag{16}$$

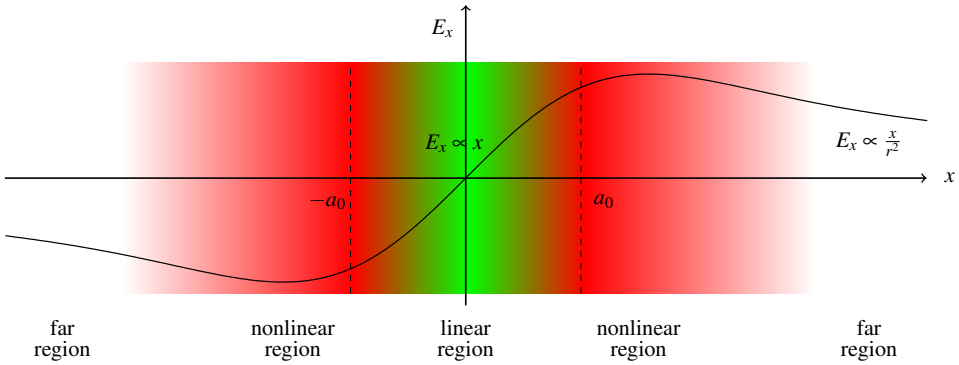


**Fig. 5:** Electric field generated by a 2D Gaussian particle distribution. For comparison, in the linear region the gradient is the same of that of Fig. 4. The green area is the region of linear electric field. It is clear that the stronger electric field is not found at $\pm a_0$.

with $r^2 = x^2 + y^2$, and by making the variable substitution $r' = ra_0/\sqrt{a_0^2 + t}$, we obtain Eq. (12).

According to the particle amplitude, we distinguish the electric field in three regions: (1) a linear region close to the beam centre; (2) a non-linear region, characterized by a significant change in the electric field in a non-linear way; (3) a far region characterized by a functional dependence as $1/r$. This third dependence is valid for $a_0, b_0 \ll r \ll R$, with $R$ the radius of the accelerator. This characterization of the electric field is shown in Fig. 5.

## 5 Dynamics in the linear region

The previous section has helped to characterize the electric field generated in the transverse section of a 2D matched beam. The way in which the discussion has been developed assumes that the beam does not change as a result of space charge; hence, the matched beam distribution is following the optics, and does not change for other reasons. We call this distribution 'frozen'. The $x$–$y$ projection of the frozen beam at the longitudinal position $s$ always creates an ellipsoidal beam distribution described by Eq. (10). We now discuss the effect of the electric field on a particle with a trajectory that remains close to the beam centre. This means that, at any instant during the transport, the co-ordinates $x, y$ of this particle should satisfy the condition $|x|, |y| \ll a_0, b_0$. This condition simplifies Eq. (14). In fact, $\hat{T}$ as defined by Eq. (15) will always satisfy $\hat{T} \leq x^2/a_0^2 + y^2/b_0^2$ for any $t \geq 0$. As $|x|, |y| \ll a_0, b_0$, it follows that $\hat{T}$ will always be very small; hence, to a good approximation, we can replace $\hat{T} = 0$. We therefore find that for $|x|, |y| \ll a_0, b_0$ the electric field is

$$E_x = \frac{\lambda \hat{n}(0)}{2\pi\varepsilon_0} x \int_0^\infty \frac{1}{(a_0^2 + t)^{3/2}(b_0^2 + t)^{1/2}} \mathrm{d}t \,,$$

and the integral is readily evaluated, with the result:

$$E_x = \frac{\lambda \hat{n}(0)}{\pi\varepsilon_0} \frac{1}{a_0(a_0 + b_0)} x \,. \tag{17}$$

This equation says that all the 2D matched frozen distributions create linear forces in the proximity of the origin. The influence on the type of beam distribution appears in the term $\hat{n}(0)$. This quantity changes value according to whether the distribution is Kapchinsky–Vladimirsky, waterbag, or Gaussian. We notice that the electric field in the proximity of the beam centre acts like a defocusing element distributed along the ring.

As we are considering a 'frozen' beam, that is, a beam with sizes following the machine optics, we can at this stage consider the electric force generated by the beam as 'external', just as if it is applied

to the beam particles from a sort of a distributed quadrupole. It therefore makes perfect sense to consider what the single-particle dynamics would be in the presence of such a force.

We remind ourselves here that the single-particle dynamics of a particle in a lattice and in the presence of space charge is

$$\frac{\mathrm{d}^2x}{\mathrm{d}s^2} + k_{0x}(s)x = \frac{q}{m\gamma^3 v_s^2}E_x\,, \tag{18}$$

where $k_{0x}(s)$ is the horizontal focusing or defocusing strength exerted by the magnets on one charged particle with charge $q$ and mass $m$, $\gamma = 1/\sqrt{1-v_s^2/c^2}$, and $v_s$ is the speed of the particle. $E_x$ is the Coulomb electric field, and the term $\gamma^3$ includes the effect of the self-magnetic field, which, at high energies, compensates the space charge. If we substitute the electric field close to the origin (Eq. (17)) in the equation of motion (Eq. (18)), then the equation of motion becomes a Hill equation that includes the effect of the linear space charge. This happens in the centre of the beam under the assumption that the beam is coasting, ellipsoidal, and frozen. It is convenient to incorporate all constants in one single coefficient called the perveance, defined as

$$K = \frac{qI}{2\pi\varepsilon_0 m\gamma^3\beta^3c^3}\,, \tag{19}$$

where $I$ is the beam current, and $\beta = v_z/c$. In the following, we take $K$ to be always positive. The equations of motion of the single particle then become

$$\frac{\mathrm{d}^2x}{\mathrm{d}s^2} + \left[k_{0x}(s) - \hat{n}(0)\frac{2K}{a_0(a_0+b_0)}\right]x = 0\,, \tag{20}$$

$$\frac{\mathrm{d}^2y}{\mathrm{d}s^2} + \left[k_{0y}(s) - \hat{n}(0)\frac{2K}{b_0(a_0+b_0)}\right]y = 0\,. \tag{21}$$

As previously stated, these are the equations of motion for a particle in the centre of a coasting beam. The 2D beam distribution is defined by the Eq. (5), the $x$–$y$ projection of which is given by Eq. (9). In this discussion, the beam distribution is 'frozen', i.e., the type of distribution does not change, and the sizes $a_0, b_0$ are 'matched' with the machine optics as $a_0 = \sqrt{\beta_{0x}\mathscr{E}_x}$ and $b_0 = \sqrt{\beta_{0y}\mathscr{E}_y}$. Now we can discuss the optics that a particle will experience in the presence of frozen space charge when its motion is close the origin. From Eqs. (20) and (21), we find that the effective strength of the lattice is now:

$$\begin{aligned} k_{1x}(s) =& k_{0x}(s) - \hat{n}(0)\frac{2K}{a_0(a_0+b_0)}\,,\\ k_{1y}(s) =& k_{0y}(s) - \hat{n}(0)\frac{2K}{b_0(a_0+b_0)}\,. \end{aligned} \tag{22}$$

These two strengths are well defined, and produce the modified optical function $\beta_{1x}, \alpha_{1x}, \beta_{1y}, \alpha_{1y}$. Again, we observe that the memory of the type of distribution is in the factor $\hat{n}(0)$, and the size of the distribution is related to $a_0(s), b_0(s)$.

## 6 Frozen beam matched with space charge

If we consider the modified lattice in Eq. (22), we are obliged to admit that the effective strengths $k_{1x}, k_{1y}$ will create a different optics from the original lattice. Once we fix $\mathscr{E}_x, \mathscr{E}_y$, given the optics $\beta_{0x}, \alpha_{0x}, \beta_{0y}, \alpha_{0y}$, the frozen beam distribution creates, in the centre of the beam, via space charge, the modified optics $\beta_{1,x}, \alpha_{1,x}, \beta_{1,y}, \alpha_{1,y}$, and this new optics is periodic, as originated by periodic functions: the effect of the frozen space charge is to modify the Twiss parameters.

We could now think to create a beam distribution, which is matched with the optics created by the space charge depressed strength $k_{1x}, k_{1y}$. This beam will have the following frozen distribution matched with the new optics

$$\frac{1}{\pi^2 \mathscr{E}_x \mathscr{E}_y} \tilde{n} \left( \frac{\varepsilon_{1x}}{\mathscr{E}_x} + \frac{\varepsilon_{1y}}{\mathscr{E}_y} \right), \tag{23}$$

where the Courant–Snyder quantities $\varepsilon_{1x}, \varepsilon_{1y}$ are now constructed using the modified optical functions $\beta_{1x}, \alpha_{1x}, \beta_{1y}, \alpha_{1y}$, namely

$$\begin{aligned} \varepsilon_{1x} &= \beta_{1x} x'^2 + 2\alpha_{1x} x x' + \gamma_{1x} x^2 , \\ \varepsilon_{1y} &= \beta_{1y} y'^2 + 2\alpha_{1y} y y' + \gamma_{1y} y^2 . \end{aligned} \tag{24}$$

At this point it is clear that Eqs. (23) and (5) represent two distinct distributions, because the same distribution function makes use of two distinct sets of optics.

To achieve a more realistic modelling of the matching of a 2D intense particle beam, it is necessary that 'both the beam distributions' are the same. This, in fact, is what happens in the real machine: the machine optics is changed by the beam distribution, which in turn 'automatically' guides the beam evolution and creates the same optics. In other words, the matched 2D beam, including space charge, requires the creation of a frozen beam distribution with an optics that already include the effect of that space charge. The problem is that we do not know in advance the modified optics with space charge. Mathematically this means finding $\beta_x, \alpha_x, \beta_y, \alpha_y$ such that $a = \sqrt{\mathscr{E}_x \beta_x}, b = \sqrt{\mathscr{E}_y \beta_y}$ creates a depressed focusing strength

$$\begin{aligned} k_x(s) &= k_{0x}(s) - \hat{n}(0) \frac{2K}{a(a+b)} , \\ k_y(s) &= k_{0y}(s) - \hat{n}(0) \frac{2K}{b(a+b)} , \end{aligned} \tag{25}$$

which in turns creates exactly $\beta_x, \alpha_x, \beta_y, \alpha_y$. The solution to this problem is not obvious and must be discussed with care, according to the circumstances.

Practically, one starts from a 'naked' optics $\beta_{0x}, \alpha_{0x}, \beta_{0y}, \alpha_{0y}$, from which one finds the frozen beam sizes $a_0, b_0$. Using Eq. (22), we find new optics $\beta_{1,x}, \alpha_{1,x}, \beta_{1,y}, \alpha_{1,y}$. The new modified optics includes the space charge in an 'inconsistent' fashion. However, if the space charge is not too strong, the modified optics is closer than the naked one to the solution. Therefore, we can repeat the process, now creating another frozen beam, matched with the optics $\beta_{1,x}, \alpha_{1,x}, \beta_{1,y}, \alpha_{1,y}$, from which we compute the new beam sizes $a_1, b_1$ and again, using an equation similar to Eq. (22), we find a new optics $\beta_{2,x}, \alpha_{2,x}, \beta_{2,y}, \alpha_{2,y}$. This procedure of steps defines an infinite sequence by recursion:

$$\beta_{n,x}, \alpha_{n,x}, \beta_{n,y}, \alpha_{n,y} \longrightarrow \beta_{n+1,x}, \alpha_{n+1,x}, \beta_{n+1,y}, \alpha_{n+1,y} ,$$

which starts from $\beta_{0x}, \alpha_{0x}, \beta_{0y}, \alpha_{0y}$. If the sequence converges, the limit is our $\beta_x, \alpha_x, \beta_y, \alpha_y$, which satisfies Eq. (25). Practically if the sequence converges, an adequate approximation is reached in a relatively small number of iterations.

## 7 Stationary distributions

Till now we have treated the space charge created by a frozen beam. That is, a beam of the sizes which are frozen to the beam optics; in the last section, we found that it is closer to the reality if the frozen beam is matched with the optics that include the space charge (generated by the beam itself). However, another assumption has been implicitly used: we always assumed that the type of distribution remains

the same during the beam evolution. In the framework of the frozen beams, this is perfectly allowed. We now discuss what happens if we allow all particles to evolve according to the actual electric field, in a self-consistent way. We basically want to discuss the evolution of the complete beam. In general, our 'matched' distribution will evolve in a very complex way. If the mechanisms that lead to beam change are slow on the time-scale under consideration, we can assume that the distribution will remain matched, i.e., it keeps a form type

$$n(x,x',y,y',s) = \frac{1}{\pi^2 \mathscr{E}_x \mathscr{E}_y} \tilde{n}\left(\frac{\varepsilon_x}{\mathscr{E}_x} + \frac{\varepsilon_y}{\mathscr{E}_y}, s\right),$$

where the appearance of the variable $s$ in the function describing the beam distribution means that the type of distribution may change with time, for example a Kapchinsky–Vladimirsky distribution may change and become a Gaussian. In complete generality, the evolution of a particle distribution is ruled by the Vlasov equation. For convenience, let us call $\vec{v} = (x,x',y,y')$; the Liouville theorem states that:

$$\frac{\partial}{\partial s} n(\vec{v},s) + \sum_i v_i' \frac{\partial}{\partial v_i} n(\vec{v},s) = 0 \tag{26}$$

except that now the quantities $v_i'$ are obtained from the canonical equations, which read:

$$v_i' = S_{ij} \frac{\partial}{\partial v_j} H(\vec{v}), \tag{27}$$

with

$$S = \begin{pmatrix} 0 & 1 & 0 & 0 \\ -1 & 0 & 0 & 0 \\ 0 & 0 & 0 & 1 \\ 0 & 0 & -1 & 0 \end{pmatrix},$$

and $H(\vec{v})$ the Hamiltonian of the system.

Equations (26) and (27), jointly, form the Vlasov equation, which, in its explicit form, reads:

$$\frac{\partial n}{\partial s} + (\vec{\nabla} n) \cdot (S\vec{\nabla} H) = 0.$$

Note that, with space charge, the Liouville theorem is still applicable if bulk space charge and beam currents can be described by vector potentials $\phi, \vec{A}$ (see Ref. [3]).

This equation tells how the particle density, i.e., the function $n$, changes in time. This is expressed by the dependence on $s$, which, where it exists, yields $\frac{\partial}{\partial s} n(\vec{v},s) \neq 0$. If, instead,

$$\frac{\partial}{\partial s} n(\vec{v},s) = 0,$$

this means that the particle distribution does not depend on $s$; hence, it does not change 'shape' with time. In the absence of space charge, or with very small space charge, the general particle distribution

$$\tilde{n}\left(\frac{\varepsilon_{0x}(x,x',s)}{\mathscr{E}_x} + \frac{\varepsilon_{0y}(y,y',s)}{\mathscr{E}_y}, s\right)$$

is stationary. In fact, it is easy to check that, in the absence of space charge,

$$\frac{\partial}{\partial s} \tilde{n}\left(\frac{\varepsilon_{0x}(x,x',s)}{\mathscr{E}_x} + \frac{\varepsilon_{0y}(y,y',s)}{\mathscr{E}_y}, s\right) = 0.$$

In the presence of space charge, the situation is much more complicated. There is only one known distribution that is stationary with space charge and that is the Kapchinsky–Vladimirsky distribution. In fact, for the Kapchinsky–Vladimirsky distribution,

$$n(\vec{v},s) = \frac{1}{\pi^2 \mathscr{E}_x \mathscr{E}_y} \delta\left(\frac{\varepsilon_x}{\mathscr{E}_x} + \frac{\varepsilon_y}{\mathscr{E}_y} - 1\right), \tag{28}$$

if used in Eq. (9), we find that the function $F(t)$ becomes $F(t) = \Theta(t-1)$, where the function $\Theta(u)$ has value $\Theta(u) = 0$ if $u < 0$, and $\Theta(u) = 1$ if $u > 0$. Therefore, we find

$$n(x,y) = \frac{1}{\pi ab}\left[1 - \Theta\left(\frac{x^2}{a^2} + \frac{y^2}{b^2} - 1\right)\right] = \frac{1}{\pi ab}\Theta\left(1 - \frac{x^2}{a^2} - \frac{y^2}{b^2}\right),$$

which simply means that if $(x,y)$ is inside the beam, i.e., if

$$\frac{x^2}{a^2} + \frac{y^2}{b^2} \leq 1,$$

the projection of the beam on the $x$–$y$ plane has constant density $n(x,y) = 1/(\pi ab)$; if $(x,y)$ is outside the beam, then $n(x,y) = 0$, as one expects. As $n(x,y)$ is constant, we find that the electric fields are linear everywhere inside the beam. In fact, Eq. (14) specialized to the Kapchinsky–Vladimirsky distribution yields

$$E_x = \frac{\lambda}{2\pi\varepsilon_0} x \int_0^\infty \frac{1}{(a_0^2+t)^{3/2}(b_0^2+t)^{1/2}} \mathrm{d}t \tag{29}$$

for any $(x,y)$ inside the beam, and by direct integration we find

$$E_x = \frac{\lambda}{\pi\varepsilon_0} x \frac{1}{a_0(a_0+b_0)}.$$

Similarly, for the $y$ plane. We therefore find that the Kapchinsky–Vladimirsky distribution creates a linear electric field everywhere inside the beam. This electric field enters the Hill's equation, and consequently the optics with space charge can be obtained. But now it is straightforward to prove that, for the particle distribution in Eq. (28), we find

$$\sum_i v_i' \frac{\partial}{\partial v_i} n(\vec{v},s) + \frac{\partial n}{\partial \varepsilon_x}\frac{\partial \varepsilon_x}{\partial s} + \frac{\partial n}{\partial \varepsilon_y}\frac{\partial \varepsilon_y}{\partial s} = 0,$$

which implies that

$$\frac{\partial}{\partial s} n\left(\frac{\varepsilon_x(x,x',s)}{\mathscr{E}_x} + \frac{\varepsilon_y(y,y',s)}{\mathscr{E}_y}, s\right) = 0,$$

that is the Kapchinsky–Vladimirsky is a stationary distribution. (The partial derivative is applied only to the last $s$, i.e., to the functional dependence of the type of distribution). All this means that any initial Kapchinsky–Vladimirsky distribution will remain a Kapchinsky–Vladimirsky distribution, that is, this distribution will not change shape during the beam evolution.

Next, we show an example of evolution of a non-stationary beam distribution. In Fig. 6, we see in green the $y$ profile of a Kapchinsky–Vladimirsky distribution. This distribution is injected into a lattice with $Q_{0x} = Q_{0y} = 4.41$ with emittances $\tilde{\varepsilon}_x = \tilde{\varepsilon}_y = 5$ mm-mrad. A mismatch of $M = 30\%$ is applied in both planes. This means that the $x$ co-ordinates are multiplied by 1.3, and the $x'$ co-ordinates are divided by 1.3, leaving the emittance unchanged, and likewise for the $y$ plane. (The space charge tune-shift is $\Delta Q_x = -0.165$). The distribution is left circulating in a ring for 200 turns, and afterwards the beam profile is shown by the black curve. The particle-in-cell simulation clearly shows that the beam distribution changes shape and readjusts to a different type.

## 8 Beam characterization

Unless something dramatic happens to the beam, the beam distribution does not change too quickly. Therefore, for a short time-scale, one can ask on how a beam distribution can be characterized.

Experimentally, this task is very difficult, as it necessitates a complete 4D phase space reconstruction, and in circular machines only the measurement of beam profiles is part of normal diagnostics, or the application of 2D tomographic techniques.

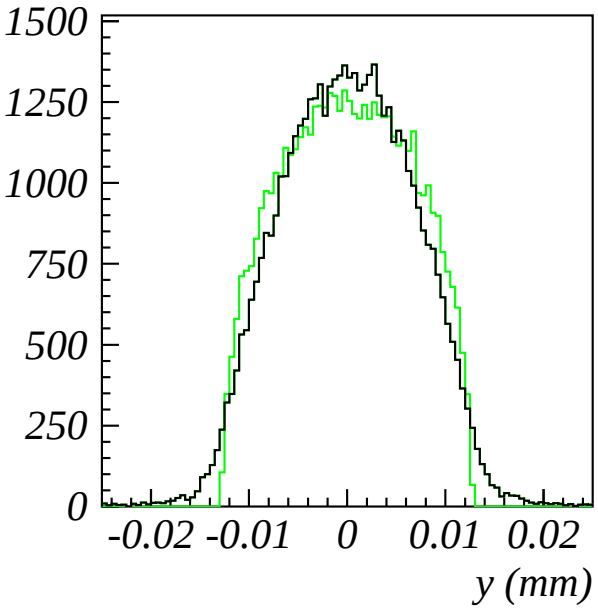


**Fig. 6:** Evolution of non-stationary beam distribution as obtained from a particle-in-cell simulation

From the point of view of multiparticle simulations, at each step of a simulation, the full multi-particle beam distribution is accessible, and a characterization of the beam is useful. The easier way to characterize the beam is through the second-order moments. If the centre of mass of the beam is in the origin, i.e., if $\sum_{i=1}^{N} x_i = \sum_{i=1}^{N} x_i' = \sum_{i=1}^{N} y_i = \sum_{i=1}^{N} y_i' = 0$, with $N$ the total number of macro-particles, the second-order moments

$$\begin{aligned} \langle x^2 \rangle &= \frac{1}{N}\sum_{i=1}^{N} x_i^2 , \\ \langle x'^2 \rangle &= \frac{1}{N}\sum_{i=1}^{N} x_i'^2 , \\ \langle xx' \rangle &= \frac{1}{N}\sum_{i=1}^{N} x_i x_i' \end{aligned} \tag{30}$$

enable the following quantities to be defined: the r.m.s. beam size $\tilde{x}$ is defined as

$$\tilde{x} = \sqrt{\langle x^2 \rangle} ,$$

and the r.m.s. beam emittance $\tilde{\varepsilon}_x$ is defined as

$$\tilde{\varepsilon}_x = \sqrt{\langle x^2 \rangle \langle x'^2 \rangle - \langle xx' \rangle^2} .$$

Similar moments and definitions apply for the $y$ plane.

For matched beams, as we defined in this paper, there is a direct relation between the quantities $\mathscr{E}_x, \mathscr{E}_y$, the beam distribution type, and second order moments. By assuming that the 2D beam distribution has the general analytic shape

$$n(x,x',y,y') = \frac{1}{\pi^2 \mathscr{E}_x \mathscr{E}_y} \tilde{n}\left( \frac{\varepsilon_{0x}(x,x',s)}{\mathscr{E}_x} + \frac{\varepsilon_{0y}(y,y',s)}{\mathscr{E}_y} \right)$$

**Table 2:** Main properties of the three types of distribution. For KV, and WB distribution, the spatial distribution $n(x,y)$ is meant in the domain $x^2/a^2+y^2/b^2\leq 1$.

| | $n(x,x',y,y')$ | $n(x,y)$ | $a/\tilde{x}$ | $\mathscr{E}_x/\tilde{\varepsilon}_x$ |
|---|---|---|---|---|
| Kapchinsky–Vladimirsky | $\frac{1}{\pi^2\mathscr{E}_x\mathscr{E}_y}\delta\left(\frac{\varepsilon_x}{\mathscr{E}_x}+\frac{\varepsilon_y}{\mathscr{E}_y}-1\right)$ | $\frac{1}{\pi ab}$ | 2 | 4 |
| Waterbag | $\frac{2}{\pi^2\mathscr{E}_x\mathscr{E}_x}\Theta\left(1-\frac{\varepsilon_x}{\mathscr{E}_x}-\frac{\varepsilon_y}{\mathscr{E}_y}\right)$ | $\frac{2}{\pi ab}\left(1-\frac{x^2}{a^2}-\frac{y^2}{b^2}\right)$ | $\sqrt{6}$ | 6 |
| Gaussian | $\frac{1}{4\pi^2\mathscr{E}_x\mathscr{E}_y}\exp\left[-\frac{1}{2}\left(\frac{\varepsilon_x}{\mathscr{E}_x}+\frac{\varepsilon_y}{\mathscr{E}_y}\right)\right]$ | $\frac{1}{2\pi ab}\exp\left[-\frac{1}{2}\left(\frac{x^2}{a^2}+\frac{y^2}{b^2}\right)\right]$ | 1 | 1 |

and ignoring at this point the possible $s$ dependence of the type of distribution, we find characteristic relations between r.m.s. sizes $\tilde{x},\tilde{y}$, and sizes $a,b$, also between $\mathscr{E}_x,\mathscr{E}_y$ and the r.m.s. emittances $\tilde{\varepsilon}_x,\tilde{\varepsilon}_y$. These relations are shown in Table 2 for the three types of distribution here presented. The ratios $a/\tilde{x}$, and $\mathscr{E}_x/\tilde{\varepsilon}_x$ are important; in fact, we see that the relation between the edge of a beam and the r.m.s. size depends on the type of distribution that we are dealing with.

## 9 Envelope equation

As discussed in the previous section, the Kapchinsky–Vladimirsky distribution is stationary, that is, a Kapchinsky–Vladimirsky distribution will evolve while remaining a Kapchinsky–Vladimirsky type. From the previous section, we find that, once the type of a certain matched distribution is known, we need to know only two parameters to completely define all its properties. These parameters can be $\mathscr{E}_x,\mathscr{E}_y$, or $a,b$. Alternatively, r.m.s. quantities are also helpful to find these two parameters, for example, $\tilde{\varepsilon}_x,\tilde{\varepsilon}_y$, or $\tilde{x},\tilde{y}$.

For linear lattices, the Kapchinsky–Vladimirsky distribution is stationary; hence, we can describe the evolution of the beam distribution by characterizing the evolution of the chosen parameters. The r.m.s. emittances have the interesting property that they remain constant under linear forces. In fact, from the definition $\tilde{\varepsilon}_x^2=\langle x^2\rangle\langle x'^2\rangle-\langle xx'\rangle^2$, it is easy to verify that

$$\frac{\mathrm{d}\tilde{\varepsilon}_x^2}{\mathrm{d}s}=\frac{\mathrm{d}}{\mathrm{d}s}(\langle x'^2\rangle\langle x^2\rangle-\langle xx'\rangle^2)=2(\langle x'x''\rangle\langle x^2\rangle-\langle xx'\rangle\langle xx''\rangle)\,. \tag{31}$$

If the forces acting on each particle are linear; hence, if the equation of motion is $x''=\xi(s)x$ with $\xi(s)$ an arbitrary function, then using it in Eq. (31) yields $\mathrm{d}\tilde{\varepsilon}_x^2/\mathrm{d}s=0$.

Therefore, for linear forces $\tilde{\varepsilon}_x$ cannot be used to describe the evolution of the beam. We have to consider the r.m.s. beam sizes instead. From the definition of $\tilde{x}$ we find

$$\tilde{x}'=\frac{\langle xx'\rangle}{\tilde{x}}$$

and

$$\tilde{x}''=\frac{\langle xx''\rangle\tilde{x}^2+\langle x'^2\rangle\tilde{x}^2-\langle xx'\rangle^2}{\tilde{x}^3}\,. \tag{32}$$

By using the definition of the r.m.s. emittance, we find

$$\tilde{x}''=\frac{\langle xx''\rangle}{\tilde{x}}+\frac{\tilde{\varepsilon}_x^2}{\tilde{x}^3}\,. \tag{33}$$

As the equations of motion are linear,

$$\frac{\mathrm{d}^2x}{\mathrm{d}s^2}+\left[k_{0x}(s)-\frac{2K}{a(a+b)}\right]x=0\,, \tag{34}$$

we then find

$$\tilde{x}'' + k_{0x}(s)\tilde{x} - \frac{2K}{a(a+b)}\tilde{x} - \frac{\tilde{\varepsilon}_x^2}{\tilde{x}^3} = 0\,.$$

As we are discussing a Kapchinsky–Vladimirsky distribution, we can rewrite $a, b$ as functions of the r.m.s. sizes and find

$$\tilde{x}'' + k_{0x}(s)\tilde{x} - \frac{K}{2(\tilde{x}+\tilde{y})} - \frac{\tilde{\varepsilon}_x^2}{\tilde{x}^3} = 0\,.$$

A similar equation holds for the $y$ plane inverting $\tilde{x} \leftrightarrow \tilde{y}$. The fact that $\tilde{\varepsilon}_x$ and $\tilde{\varepsilon}_y$ are constant for a Kapchinsky–Vladimirsky distribution allows to use the r.m.s. envelope equations,

$$\tilde{x}'' + k_{0x}(s)\tilde{x} - \frac{K}{2(\tilde{x}+\tilde{y})} - \frac{\tilde{\varepsilon}_x^2}{\tilde{x}^3} = 0\,, \tag{35}$$

$$\tilde{y}'' + k_{0y}(s)\tilde{y} - \frac{K}{2(\tilde{x}+\tilde{y})} - \frac{\tilde{\varepsilon}_y^2}{\tilde{y}^3} = 0\,, \tag{36}$$

$$\tag{37}$$

to predict the evolution of $\tilde{x}, \tilde{y}$. As the Kapchinsky–Vladimirsky distribution does not change type, we can compute the evolution of the envelopes $a, b$, as $a = 2\tilde{x}, b = 2\tilde{y}$.

## 10 R.m.s. equivalent beams

If the time-scales considered are short enough, so that the distribution does not significantly change type, we can wonder if there exists a generalization of the r.m.s. envelope equations. We face here the problem of how to describe the evolution of a non-Kapchinsky–Vladimirsky distribution, which, therefore, necessarily yields non-linear space charge forces. We start here with the assumption that the beam distribution, i.e., the type of distribution, does not change. Again, the evolution of the beam is described by the two quantities that characterize the beam. The evolution of the r.m.s. moments requires evaluation of the quantity $\langle xx'' \rangle$ in Eq. (32), but now the equation of motion of a single particle becomes

$$\frac{\mathrm{d}^2 x}{\mathrm{d}s^2} + k_{0x}(s)x - Kx\int_0^\infty \frac{\hat{n}(\hat{T})}{(a^2+t)^{3/2}(b^2+t)^{1/2}}\mathrm{d}t = 0\,, \tag{38}$$

$$\tag{39}$$

where $\hat{T}$ is given by Eq. (15). Therefore,

$$\langle xx'' \rangle = -k_{0x}\langle x^2 \rangle + K\left\langle x^2 \int_0^\infty \frac{\hat{n}(\hat{T})}{(a^2+t)^{3/2}(b^2+t)^{1/2}}\mathrm{d}t \right\rangle ,$$

and the last term becomes rather complicated to compute. However, Sacherer has proved [4] that for the class of beam distributions

$$\rho = \lambda \frac{1}{\pi ab}\hat{n}\left(\frac{x^2}{a^2} + \frac{y^2}{b^2}\right) ,$$

which are our matched beams, the following remarkable result holds:

$$K\left\langle x^2 \int_0^\infty \frac{\hat{n}(\hat{T})}{(a^2+t)^{3/2}(b^2+t)^{1/2}}\mathrm{d}t \right\rangle = \frac{K}{2}\frac{\tilde{x}}{\tilde{x}+\tilde{y}}\,.$$

This is valid independently of the function $\hat{n}(t)$. Therefore, Eq. (33) becomes

$$\tilde{x}'' = -k_{0x}(s)\tilde{x} + \frac{K}{2}\frac{1}{\tilde{x}+\tilde{y}} + \frac{\tilde{\varepsilon}_x^2}{\tilde{x}^3}\,. \tag{40}$$

This equation shows that the effect of the space charge in the term $\langle xx'' \rangle$ has always the same functional form, as for a Kapchinsky–Vladimirsky beam. This result is remarkable because it means that, independently of the type of beam distribution, if a beam is matched and the distribution type does not change, the r.m.s. envelope will evolve in the same way: this also means that if two beams have the same r.m.s. moments at given $s$, their r.m.s. envelopes will evolve in the same manner. These beams are called *r.m.s. equivalent*.

Clearly, this result is valid as long as the type of distribution does not change. If the r.m.s. emittance does not change, then the equations can be directly integrated; however, if r.m.s. emittance changes, it is then necessary to provide its evolution, as Eq. (40) alone will not be sufficient to predict the evolution of $\tilde{x}$.

## 11 Incoherent tune-shift

The tune of a single particle for a linear machine is defined as

$$Q_{0x} = \frac{1}{2\pi}\int_0^L \frac{1}{\beta_{0x}(s)}\mathrm{d}s\,,$$

and the Courant–Snyder theory shows that a localized gradient error of integrated strength $\Delta k_x$ produces a change of tune as

$$\Delta Q_{0x} = \frac{1}{4\pi}\beta_{0x}(s)\Delta k_x\,.$$

The space charge in the centre of a beam acts exactly as a small defocusing gradient error. If a particle has small transverse amplitude (i.e., is mainly close to the beam centre), then the effect of the space charge on this particle when it goes from $s$ to $s+\Delta s$, is given a local kick

$$\Delta x' = \hat{n}(0)\frac{2K}{a(s)[a(s)+b(s)]}x\Delta s\,,$$

in the same way, a local gradient $\Delta k_x$ produces a kick $\Delta x' = -\Delta k_x x$. The positive sign of the kick stems from the space charge force, which is always defocusing. Therefore, the change of tune is then

$$\Delta Q_{0x} = -\frac{1}{4\pi}\beta_{0x}(s)\hat{n}(0)\frac{2K}{a(s)[a(s)+b(s)]}\Delta s\,.$$

By integration of all the distributed effect of space charge along the circumference, we obtain

$$\Delta Q_{0x} = -\frac{1}{4\pi}\int_0^L \beta_{0x}(s)\hat{n}(0)\frac{2K}{a(s)[a(s)+b(s)]}\mathrm{d}s\,.$$

Now we rewrite this equation as

$$\Delta Q_{0x} = -\frac{1}{4\pi}\frac{1}{\mathscr{E}_x}\int_0^L \frac{\beta_{0x}(s)}{\beta_x(s)}\hat{n}(0)\frac{2K}{1+\sqrt{\frac{\mathscr{E}_y\beta_y(s)}{\mathscr{E}_x\beta_x(s)}}}\mathrm{d}s\,.$$

If the space charge is not too strong, then $\beta_{0x}/\beta_x(s) \simeq 1$, and

$$\Delta Q_{0x} = -\frac{1}{4\pi}\frac{1}{\mathscr{E}_x}\hat{n}(0)2K2\pi R\left\langle \frac{1}{1+\sqrt{\frac{\mathscr{E}_y\beta_y(s)}{\mathscr{E}_x\beta_x(s)}}}\right\rangle_s\,,$$

where $\langle\rangle_s$ is the average over the machine length, and $R$ is the average machine radius.

We next consider the decomposition of the beta functions around their average $\langle\beta_x\rangle_s$, and $\langle\beta_y\rangle_s$, as

$$\begin{aligned}\beta_x(s) &= \langle\beta_x\rangle_s + \Delta\beta_x(s)\,,\\ \beta_y(s) &= \langle\beta_y\rangle_s + \Delta\beta_y(s)\,,\end{aligned} \tag{41}$$

and we also consider the following auxiliary function

$$\mathscr{A}(x,y) = \frac{1}{1+\sqrt{\frac{\mathscr{E}_y y}{\mathscr{E}_x x}}}\,.$$

It is clear that

$$\frac{1}{1+\sqrt{\frac{\mathscr{E}_y \beta_y(s)}{\mathscr{E}_x \beta_x(s)}}} = \mathscr{A}(\beta_x(s),\beta_y(s))\,,$$

and $\mathscr{A}$ can be Taylor expanded around $\langle\beta_x\rangle_s, \langle\beta_y\rangle_s$, as

$$\mathscr{A}(\beta_x(s),\beta_y(s)) = \sum_{n,m} \partial_x^n \partial_y^m \mathscr{A}(x,y)|_{x=\langle\beta_x\rangle_s, y=\langle\beta_y\rangle_s} \frac{[\Delta\beta_x(s)]^n [\Delta\beta_y(s)]^m}{n!m!}\,.$$

Therefore,

$$\begin{aligned}\langle\mathscr{A}(\beta_x(s),\beta_y(s))\rangle_s &= \sum_{n,m} \partial_x^n \partial_y^m \mathscr{A}(x,y)|_{x=\langle\beta_x\rangle_s, y=\langle\beta_y\rangle_s} \frac{1}{n!m!}\langle[\Delta\beta_x(s)]^n[\Delta\beta_y(s)]^m\rangle_s \\ &= \mathscr{A}(\langle\beta_x\rangle_s,\langle\beta_y\rangle_s) + O(\langle\Delta\beta_x^2\rangle_s,\langle\Delta\beta_y^2\rangle_s)\,,\end{aligned} \tag{42}$$

because by definition $\langle\Delta\beta_x\rangle_s = \langle\Delta\beta_y\rangle_s = 0$. This means that

$$\left\langle \frac{1}{1+\sqrt{\frac{\mathscr{E}_y \beta_y(s)}{\mathscr{E}_x \beta_x(s)}}} \right\rangle_s = \frac{1}{1+\sqrt{\frac{\mathscr{E}_y \langle\beta_y\rangle_s}{\mathscr{E}_x \langle\beta_x\rangle_s}}} + O(\langle\Delta\beta_x^2\rangle_s,\langle\Delta\beta_y^2\rangle_s)\,.$$

This formula states that if the beta functions do not oscillate too much away from the average beta, then we can approximate the L.H.S. with the first term of the expansion and neglect the higher order terms in $\Delta\beta_x$, and $\Delta\beta_y$. This can be seen by the second term of the expansion, which is the quadratic in the average deviation from the average beta, and which becomes small for not too wild oscillation of the beta. Therefore, under these conditions, we obtain

$$\Delta Q_{0x} = -\frac{1}{\mathscr{E}_x}\hat{n}(0)K\frac{R}{1+\sqrt{\frac{\mathscr{E}_y\langle\beta_y\rangle_s}{\mathscr{E}_x\langle\beta_x\rangle_s}}} = -\hat{n}(0)K\langle\beta_x\rangle_s\frac{R}{\sqrt{\mathscr{E}_x\langle\beta_x\rangle_s}(\sqrt{\mathscr{E}_x\langle\beta_x\rangle_s}+\sqrt{\mathscr{E}_y\langle\beta_y\rangle_s})}\,.$$

In a similar way, we can now expand the beta function in the depressed tune formula,

$$Q_x = \frac{1}{2\pi}\int_0^L \frac{1}{\beta_x(s)}\mathrm{d}s\,,$$

and we find

$$Q_x = \frac{R}{\langle\beta_x\rangle_s} + \frac{R}{\langle\beta_x\rangle_s^3}\langle\Delta\beta_x^2\rangle_s + \ldots$$

Under the same approximation of not too wild beta oscillation, we can approximate $Q_x = R/\langle\beta_x\rangle_s$, and by substitution, we finally obtain

$$\Delta Q_{0x} = -\frac{R^2}{Q_x}\hat{n}(0)K\frac{1}{\sqrt{\mathscr{E}_x\langle\beta_x\rangle_s}(\sqrt{\mathscr{E}_x\langle\beta_x\rangle_s}+\sqrt{\mathscr{E}_y\langle\beta_y\rangle_s})}\,. \tag{43}$$

This formula is very intuitive, and has a deep meaning: the incoherent space charge tune-shift appears to be insensitive to the machine optics, but to depend to an 'equivalent' smooth accelerator structure with the same tunes as the original one.

**Table 3:** Factor $f$ as function of beam distribution.

| | Kapchinsky–Vladimirsky | Waterbag | Gaussian |
|---|---|---|---|
| $f$ | 1 | 4/3 | 2 |

## 12 Space charge tune-shift for r.m.s. equivalent beams

The last formula gives the tune-shift as a function of the quantities $\mathscr{E}_x, \mathscr{E}_y$. For practical uses, it is useful to modify Eq. (43) using r.m.s. emittances. First, we observe that for a matched beam

$$\tilde{x}^2 = \mathscr{E}_x \beta_x(s) \frac{1}{2} \int_0^\infty t\hat{n}(t)\mathrm{d}t\,,$$

and the r.m.s. emittance is

$$\tilde{\varepsilon}_x = \mathscr{E}_x \frac{1}{2} \int_0^\infty t\hat{n}(t)\mathrm{d}t\,.$$

Therefore, we can rewrite the tune-shift as

$$\Delta Q_{0x} = -\frac{R^2}{Q_x}\hat{n}(0)K\frac{1}{2}\int_0^\infty t\hat{n}(t)\mathrm{d}t \frac{1}{\sqrt{\tilde{\varepsilon}_x\langle\beta_x\rangle_s}(\sqrt{\tilde{\varepsilon}_x\langle\beta_x\rangle_s}+\sqrt{\tilde{\varepsilon}_y\langle\beta_y\rangle_s})}\,,$$

and define a peak tune-shift as

$$\Delta Q_{0x} = f\Delta\tilde{Q}_{0x} \tag{44}$$

where

$$\Delta\tilde{Q}_{0x} = -\frac{R^2}{Q_x}\frac{K}{4}\frac{1}{\sqrt{\tilde{\varepsilon}_x\langle\beta_x\rangle_s}(\sqrt{\tilde{\varepsilon}_x\langle\beta_x\rangle_s}+\sqrt{\tilde{\varepsilon}_y\langle\beta_y\rangle_s})}\,, \tag{45}$$

is the tune-shift of a Kapchinsky–Vladimirsky beam r.m.s. equivalent to the beam we are considering. The factor $f$ incorporates the type of the distribution, and is

$$f = 2\hat{n}(0)\int_0^\infty t\hat{n}(t)\mathrm{d}t\,.$$

The values of $f$ according to the type of distribution are shown in Table 3. These results show that r.m.s. equivalent beams having the same perveance will produce different peak tune-shift according to the type of distribution.

## 13 Space charge limit

The previous results allow us to discuss which is the maximum current or, equivalently, the maximum number of particles a coasting beam may have in an accelerator. The limiting factor is the maximum allowed incoherent space charge tune depression, which is dictated by the necessity of avoiding the overlap of the tune-spread with machine resonances. We proceed by discussing the horizontal plane, but similar formulae are obtained on exchanging the $x$ and $y$ planes. As the resonances up to the fourth order may be dangerous for beam survival, it is then assumed that the space charge limit is set by the condition

$$|\Delta Q_{0x}| \leq |\Delta Q_{xl}| \simeq 0.25\,,$$

see Ref. [3]. This constraint can be used in Eq. (44); inverting this equation, we obtain the maximum longitudinal particle density, which reads

$$\frac{\mathrm{d}N}{\mathrm{d}s} = \frac{\lambda}{eZ} = \frac{8\pi\varepsilon_0 m_u A\gamma^3 v^2}{e^2 Z^2}\frac{|\Delta Q_{xl}|}{f}\frac{\tilde{\varepsilon}_x}{R}\left(1+\sqrt{\frac{\langle\beta_y\rangle_s\tilde{\varepsilon}_y}{\langle\beta_x\rangle_s\tilde{\varepsilon}_x}}\right)\,, \tag{46}$$

where $A$ is the mass number, $m_u$ the nucleon mass, $Z$ is the charge state of the particle, and $e$ is the elementary charge.

The same argument applies to bunched beams although we did not discuss the space charge field of a bunched beam. In fact, if a bunch is very long with respect to the transverse size, then the local coasting beam approximation enables the 'local' transverse tune-shift to be computed according to the local charge-line density $\lambda(z)$. In complete analogy, we can speak of the local current $I(z)$, which is largest where the local particle density is the largest. Therefore, one finds the peak current $I_{\text{peak}}$ in the centre of the bunch ($z = 0$). To compare how different a bunched beam is from a coasting beam, it is customary to compare the peak current of a bunched beam $I_{\text{peak}}$ with the current of a coasting beam composed of the same number of particles $I_{\text{average}}$. The ratio $B_f = I_{\text{average}}/I_{\text{peak}}$, called bunching factor, quantifies the difference between bunched beams and coasting beams. Clearly, the bunching factor is depending on the longitudinal beam distribution, and on how many bunches are accommodated in a circular machine. If $B_f = 1$ then the beam is un-bunched; the more the longitudinal bunch distribution is peaked, the smaller is $B_f$. As the largest transverse tune-spread is at the bunch centre, for that transverse section, the space charge limit is given by Eq. (46). The maximum number of particles in the ring to reach the space charge limit (hence the maximum average current), is found by multiplying Eq. (46) by $B_f$ and integrating along the circumference:

$$N_{\text{tot}} = B_f \frac{4(2\pi)^2 \varepsilon_0 m_u A \gamma^3 v^2}{e^2 Z^2} \frac{|\Delta Q_{xl}|}{f} \tilde{\varepsilon}_x \left(1 + \sqrt{\frac{\langle \beta_y \rangle_s \tilde{\varepsilon}_y}{\langle \beta_x \rangle_s \tilde{\varepsilon}_x}}\right) . \tag{47}$$

From Eq. (47), it appears evident which are the critical parameters to increase the total number of particles stored in a ring: the bunching factor $B_f$, and the type of transverse distribution, i.e., the parameter $f$. By increasing $B_f$, and making a beam closer to a Kapchinsky–Vladimirsky distribution, if possible, $N_{\text{tot}}$ will be increased. Alternatively one should compensate all natural resonances so that $|\Delta Q_{xl}|$ can be taken larger, or increase the energy of the beam to reach higher $\gamma$.

## 14 Oscillation of mismatched beams

Consider a low-intensity 2D beam matched with the machine optics at the longitudinal position $s_0$, see left panel of Fig. 7. Suppose now that we distort the beam, as shown in the right panel of Fig. 7. The black ellipse in the right panel of Fig. 7b marks the initial edge of the beam before distortion. The stretched phase space now has two 'wings', which we call A and B. If we follow the beam evolution, each particle rotates with instantaneous phase advance $1/\beta_x(s)$. While the beam moves ahead (increases $s$), the beam ellipse rotates in the co-moving reference frame preserving its area. The two beam wings out of the initial beam black ellipse, marked A and B, will also rotate as $s$ increases, as indicated by the red curved arrows.

The beam envelope is found by taking the outermost particle, and with this definition for this type of mismatched beam the envelope cannot distinguish between the two beam wings. Consequently, if the beam ellipse rotates through 180°, the two wings will swap (A $\leftrightarrow$ B), but the beam envelope will remain the same. Therefore, the beam envelope oscillates with a frequency that is the double the frequency of the single particle, i.e., the beam envelope will oscillate with a phase $2\pi(2Q_{x0})$ per turn.

This argument merely considers the single-particle dynamics, but the effect of space charge on a mismatched beam is more subtle.

To visualize the effect of the mismatch, we consider the quantity $\Delta x(s) = a(s) - a_0(s)$, where with $a_0(s)$ we indicate the matched envelope at location $s$, whereas with $a(s)$ we indicate the 'mismatched envelope' at location $s$. Figure 8 shows the evolution of $\Delta x(s)$ as obtained from a multiparticle simulation for two beams, one with low intensity (green), and one with high intensity (red). Both beams are mismatched by the same amount. The picture shows clearly that the high-intensity mismatched beam has a longer wavelength than the low-intensity one, which seems to indicate that the depressed tunes play a role in creating this shift. Therefore, at first sight, one would use the same argument as illustrated

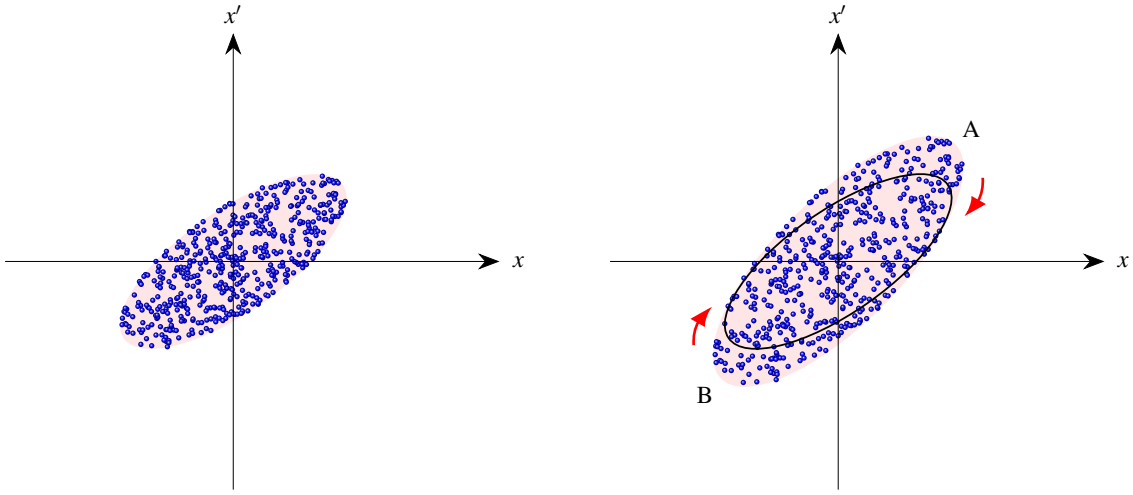


**Fig. 7:** Dynamics of mismatched beam. Left-hand side: initial matched beam distribution. Right-hand side: mismatched beam. The mismatch is produced by creating the 'wings' A and B.

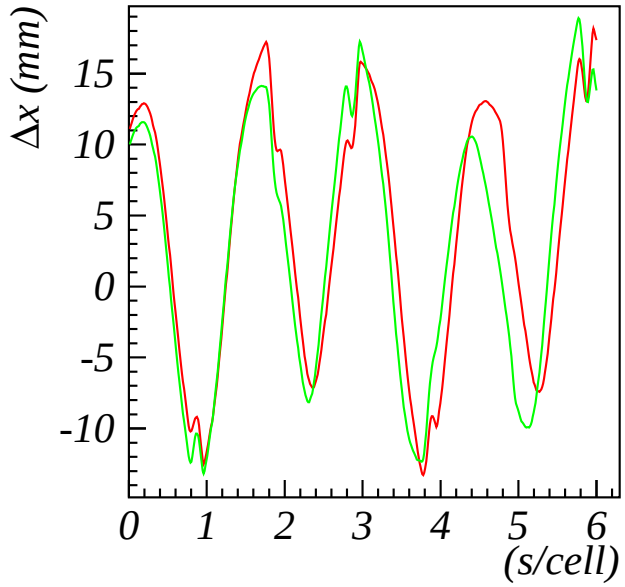


**Fig. 8:** Dynamics of mismatched beam. Green: beam with low intensity. Red: beam with high intensity

in Fig. 7 to discuss the dynamics of a mismatched high-intensity beam. As the space charge will depress the single-particle tune, one would conclude that the beam envelope will make $2Q_x$ oscillations per turn, where $Q_x$ is the depressed tune. However, this is not true.

## 15 Coherent frequencies

To explain the effect of space charge on a mismatched beam, we need to start from the envelope equations. For this discussion, it is easier to use a constant-focusing lattice, and for convenience we rescaled the r.m.s. envelope to the matched solution as $\tilde{x} = \hat{x}\tilde{x}_0, \tilde{y} = \hat{y}\tilde{y}_0$. Here $\tilde{x}_0, \tilde{y}_0$ are the r.m.s. matched

envelopes for a Kapchinsky–Vladimirsky beam with r.m.s. emittances $\tilde{\varepsilon}_x, \tilde{\varepsilon}_y$ and perveance $K$. In these terms, the envelope equations take the form

$$\hat{x}'' + k_{0x}(s)\hat{x} - \frac{K}{2}\frac{1}{\tilde{x}_0(\tilde{x}_0\hat{x}+\tilde{y}_0\hat{y})} - \frac{\tilde{\varepsilon}_x^2}{\tilde{x}_0^4\hat{x}^3} = 0\,, \tag{48}$$

$$\hat{y}'' + k_{0y}(s)\hat{y} - \frac{K}{2}\frac{1}{\tilde{y}_0(\tilde{x}_0\hat{x}+\tilde{y}_0\hat{y})} - \frac{\tilde{\varepsilon}_y^2}{\tilde{y}_0^4\hat{y}^3} = 0\,. \tag{49}$$

If $\hat{x} = \hat{y} = 1$, the beam is matched. If the beam is mismatched, then we can define $\delta\hat{x} = \hat{x} - 1$ and $\delta\hat{y} = \hat{y} - 1$, and Eqs. (48) and (49) can be expanded around the matched solution. After some algebra, and neglecting quadratic terms of the incoherent tune-shift, we find:

$$\begin{aligned} \delta\hat{x}'' + a_{xx}\delta\hat{x} + a_{xy}\delta\hat{y} = 0\,,\\ \delta\hat{y}'' + a_{yx}\delta\hat{x} + a_{yy}\delta\hat{y} = 0\,, \end{aligned} \tag{50}$$

with

$$\begin{aligned} a_{xx} &= 4\left(\frac{Q_{0x}}{R}\right)^2 - \frac{2Q_{0x}\Delta Q_x}{R^2}\left(\frac{\tilde{x}_0}{\tilde{x}_0+\tilde{y}_0} - 3\right),\\ a_{xy} &= -\frac{2Q_{0x}\Delta Q_x}{R^2}\frac{\tilde{y}_0}{\tilde{x}_0+\tilde{y}_0},\\ a_{yx} &= -\frac{2Q_{0y}\Delta Q_y}{R^2}\frac{\tilde{x}_0}{\tilde{x}_0+\tilde{y}_0},\\ a_{yy} &= 4\left(\frac{Q_{0y}}{R}\right)^2 - \frac{2Q_{0y}\Delta Q_y}{R^2}\left(\frac{\tilde{y}_0}{\tilde{x}_0+\tilde{y}_0} - 3\right). \end{aligned} \tag{51}$$

These are two linearly coupled second-order differential equations with constant coefficients. By making a proper linear co-ordinate transformation $(\delta\hat{x}, \delta\hat{y}) \to (\xi, \nu)$, the system in Eq. (50) can be decoupled into two independent differential equations,

$$\begin{aligned} \xi'' + \lambda_+\xi = 0\,,\\ \nu'' + \lambda_-\nu = 0\,, \end{aligned} \tag{52}$$

with $\lambda_\pm = Q_{\pm,\mathrm{coh}}^2/R^2$ the eigenvalues of the matrix $a_{ij}$ defining Eq. (50). For $\tilde{x}_0 \neq \tilde{y}_0$, in good approximation

$$\begin{aligned} Q_{+,\mathrm{coh}} &= 2Q_{0x} - \frac{1}{2}\Delta Q_x\left(\frac{\tilde{x}_0}{\tilde{x}_0+\tilde{y}_0} - 3\right),\\ Q_{-,\mathrm{coh}} &= 2Q_{0y} - \frac{1}{2}\Delta Q_y\left(\frac{\tilde{y}_0}{\tilde{x}_0+\tilde{y}_0} - 3\right). \end{aligned}$$

Therefore, we find that the oscillations of the envelopes around the matched solutions are obtained by the compositions of the modes with tunes $Q_{\pm,\mathrm{coh}}$ because of inverting $(\xi, \nu) \to (\delta\hat{x}, \delta\hat{y})$. We observe that $Q_{\pm,\mathrm{coh}}$ can be re-cast in a different form as

$$Q_{+,\mathrm{coh}} = 2Q_x - \frac{1}{2}\Delta Q_x\left(\frac{\tilde{x}_0}{\tilde{x}_0+\tilde{y}_0} + 1\right), \tag{53}$$

$$Q_{-,\mathrm{coh}} = 2Q_y - \frac{1}{2}\Delta Q_y\left(\frac{\tilde{y}_0}{\tilde{x}_0+\tilde{y}_0} + 1\right), \tag{54}$$

where $Q_x, Q_y$ are the depressed tunes by the incoherent space charge tune-shift, as previously discussed. These last two equations show that the modes oscillate with an extra term to the $2Q_x, 2Q_y$ which has a

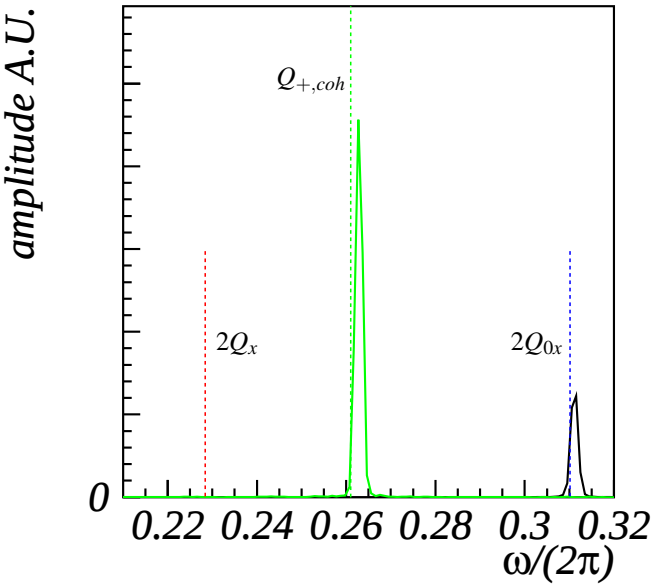


**Fig. 9:** Spectrum of oscillations of $\tilde{x}$. Black: low intensity. Green: high intensity. Dashed lines are drawn to theoretical predictions.

coherent nature, and act in the opposite direction of the incoherent tune-shift, increasing the frequency of the mode. (The sign of $\Delta Q_x, \Delta Q_y$ is negative).

Figure 9 shows the Fourier spectrum of the r.m.s. envelope of a mismatched beam. The beam is tracked in an arbitrarily chosen constant-focusing lattice of length $L = 110$ m, with tunes $Q_{0x} = 2.655, Q_{0y} = 2.823$. The incoherent space charge tune-shift is $\Delta Q_{0x} = -4 \times 10^{-2}$, $\Delta Q_y = -5.6 \times 10^{-2}$. The dashed lines show the theoretical predictions. The black spectrum is obtained by tracking a mismatched beam with no space charge, and we find it peaked on $2Q_{0x}$, as expected from the argument of the previous section. However, when the space charge is activated, the spectrum shown by the green solid curve is now peaked on the coherent frequency as predicted by the theory of Eq. (53). Note that the frequency $2Q_x$ is not excited.

This analysis is based on the r.m.s. envelope equations, and more modes of oscillation exist. A full discussion of these modes based on Vlasov equation can be found in Ref. [5]; a visual representation is shown in Fig. 10.

## 16 Tune-spread: the non-linear region

The previous analysis of the oscillations of the mismatched beam relies on the envelope equations. However, these equations do not consider the actual tune that each particle experiences. We already discussed, in Section 5, the dynamics in the linear region of the space charge field, and found a deviation of the single-particle tune from the bare tunes, which we called the incoherent space charge tune-shift $\Delta Q_{0x}, \Delta Q_{0y}$. The effect on the dynamics of the *non-linear field regime* introduced in Section 4 is still to be discussed. A first effect of the non-linear field will be to change the single-particle tunes by a different amount from $\Delta Q_{0x}, \Delta Q_{0y}$. The best way to visualize this effect is to plot, for each beam particle, its tune's deviation from the machine bare tunes. This may be computed with a standard procedure by analysing the frequency of each particle using a turn-by-turn data method [6]. The set of all these incoherent tunes is called space charge *tune-spread*. Figure 11 shows the space charge tune-spread for the three distributions presented.

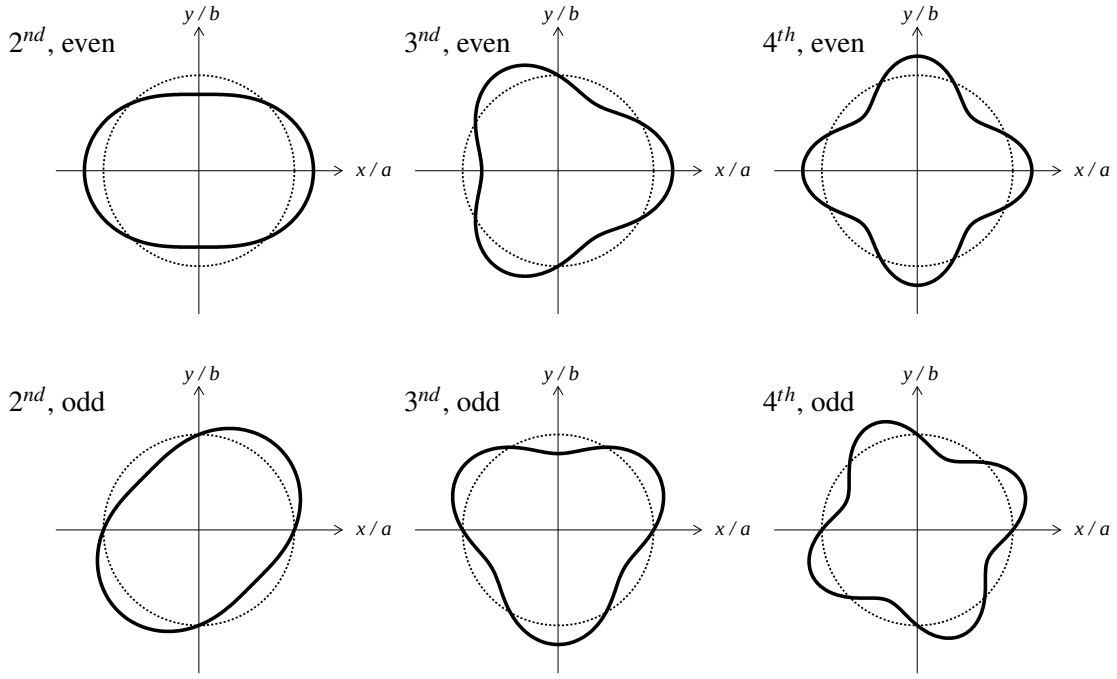


**Fig. 10:** Even and odd modes for the second, third, and fourth orders

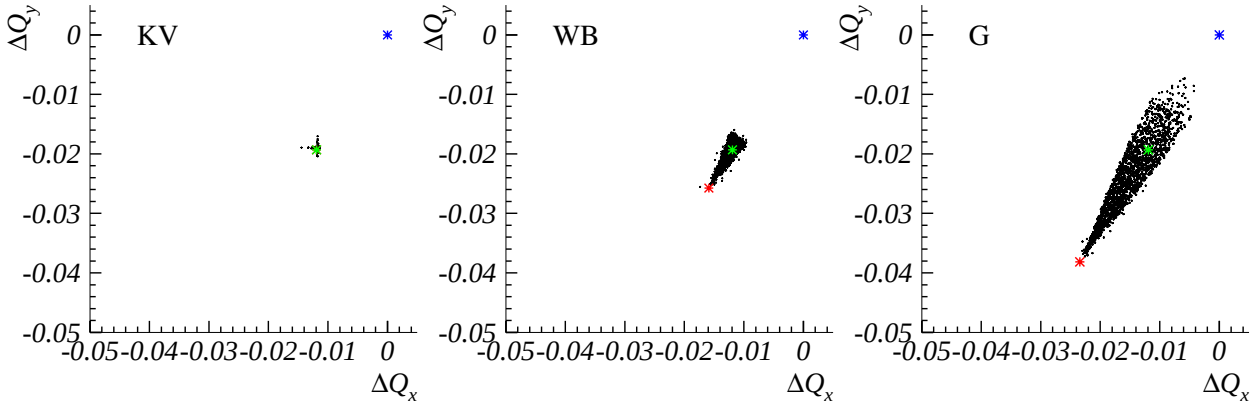


**Fig. 11:** Tune-spread of main types of particle distributions. Left-hand side: Kapchinsky–Vladimirsky (KV). Centre: waterbag (WB). Right-hand side: Gaussian (G). Blue: bare tune. Green: Kapchinsky–Vladimirsky tune-shift. Red: tune-shift for (centre) waterbag or (right-hand side) Gaussian.

The left-hand panel shows the tune-spread of a Kapchinsky–Vladimirsky distribution. Each single-particle tune is a black dot. The blue marker shows the machine bare tune, and the green marker shows incoherent detuning, as predicted by the theoretical formula of Eq. (43). The figure clearly shows that all single-particle tunes are, to a good approximation, overlapping with the theoretical tune. This happens because the electric field generated by the Kapchinsky–Vladimirsky is linear everywhere inside the beam distribution.

The panel in the centre shows the tune-spread for a 2D waterbag beam, this beam has the same perveance as the Kapchinsky–Vladimirsky beam, but the sizes are chosen so that it is r.m.s. equivalent. The set of tunes is now not overlapping and is spread over a triangular shape. The red marker shows the incoherent space charge tune-shift, as computed using Eq. (43). The factor $f$ is now 4/3, and is responsible for the increase of the tune-shift.

The panel on the right shows the space charge tune-spread for a Gaussian distribution, still r.m.s. equivalent to the Kapchinsky–Vladimirsky beam. This graph shows that the single-particle tunes are spread over a larger area, and the density of tunes decreases as the tunes approach the machine bare tune. Now $f = 2$, and the graph shows that the distance between the green and blue markers is equal to the distance between the red and the green marker.

## 17 Amplitude-dependent detuning

Figure 11 shows that all particles experience the same space charge tune-shift only for the Kapchinsky–Vladimirsky beam. For the other distributions, waterbag and Gaussian, the non-linear field creates different tunes according to how particles are distributed. It, therefore, makes sense to ask if there is any relation between the particle position and the detuning experienced by that particle. An intuitive argument helps qualitatively in understanding what happens: when a particle has a large single-particle emittance $\varepsilon_x, \varepsilon_y$, i.e., large oscillation amplitudes, this particle following the betatron motion travels periodically through the beam core and also through the beam tails; therefore, on 'average', this particle experiences a weaker electric field than those particles with small amplitudes that always stayed close the beam centre. Hence, the space charge tune-shift of a particle with large amplitudes will be smaller than $\Delta Q_{0x}, \Delta Q_{0y}$. Therefore, the larger the particle amplitude, the closer the particle tune is to the bare machine tune because it is as if the space charge is not contributing to the single-particle dynamics. In the left panel of Fig. 12, we plot all single-particle tunes of the right panel of Fig. 11 as a function of the $X$ amplitude re-scaled with the beam r.m.s. size. It can be seen that all the black dots are well contained within a red curve of simple functional dependence as

$$\Delta Q_x \simeq \Delta Q_{x,\max} \frac{1}{1 + \left(\frac{X}{2\sigma_x}\right)^2} .$$

The particle tunes are also found above the red curve, because of the vertical transverse amplitudes: even if a particle has zero horizontal amplitude, the vertical amplitude can be large, hence the horizontal transverse electric field will be diminished, with consequent reduction of the space charge tune-shift. The right-hand panel of Fig. 12 shows the tunes of a few particles with initial $\varepsilon_y \simeq 0$. These black markers overlap the red curve to good approximation.

There are more complex formulae to describe the relation between single-particle emittances (or particle action) and space charge tune-shift. For example, see Ref. [7].

## 18 Mismatched beams: free energy and emittance growth

Till now we have discussed the effect of space charge on the frequencies of particle oscillations in a beam, and on the coherent oscillation frequencies of the beam envelope. In those analyses, the starting point is from a matched beam whose properties do not change with time: this also means that all the different

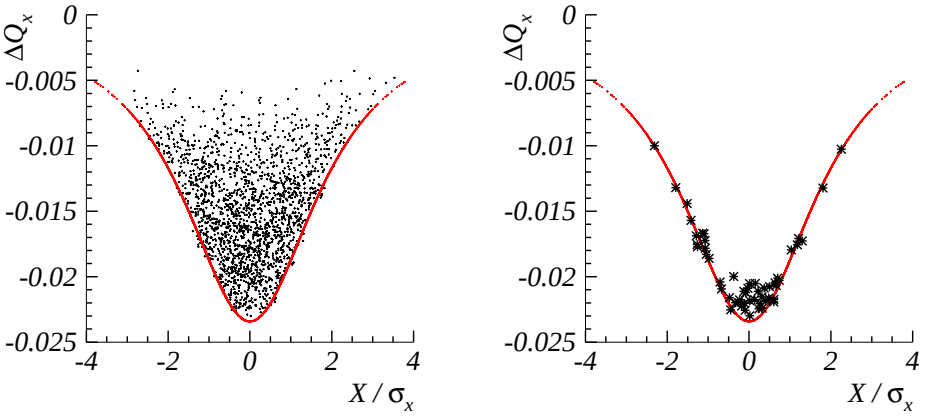


**Fig. 12:** Distribution of single-particle incoherent tune-shift in Gaussian 2D beam as function of horizontal particle amplitude. Right-hand side: only particles with $\varepsilon_y = 0$ are shown.

forms of beam energy are stationary, i.e., the beam is in 'equilibrium', and it has been assumed that any perturbation of the beam creates an oscillatory behaviour around the stationary solution. However, the possibility that the perturbation might modify the original stationary state of the beam has not been addressed.

We now discuss the possibility that, when brought out of equilibrium, a beam may evolve to a new stationary state. This discussion is developed using the concept of free energy (see in Ref. [3]). When a beam is in a stationary state, there is no free energy but when the beam is significantly perturbed, free energy is created, and this energy, assisted by other mechanisms, will re-distribute between all forms of energy, taking the beam into a new stationary state.

We make a discussion for a Kapchinsky–Vladimirsky circular beam transported in an axi-symmetric constant-focusing lattice. In this case, $\tilde{x} = \tilde{y}$ and, for convenience, we use the envelope $a = 2\tilde{x}$. As the beam is circular, we drop the index $x$ or $y$. For convenience we also use the full beam emittance $\mathscr{E} = 4\tilde{\varepsilon}$.

We recall that a stationary a beam distribution is characterized by the condition $a'' = 0$, which means

$$k_0 a - \frac{K}{a} - \frac{\mathscr{E}^2}{a^3} = 0\,.$$

It is also convenient to define the depressed focusing strengths as in Eq. (25), which now reads

$$k = k_0 - \frac{K}{a^2}\,. \tag{55}$$

We now compute the energy content of a beam when it is in a stationary state. There are three different form of energy:

1. transverse kinetic energy;
2. potential energy of particles in the potential of the lattice;
3. potential energy of the Coulomb field created by the particle distribution.

### 18.1 Transverse kinetic energy

The transverse kinetic energy of one particle is $\frac{1}{2}m\gamma(v_x^2 + v_y^2)$; therefore, the average kinetic energy of one particle is

$$E_{\rm k} = \frac{1}{2}m\gamma(\langle v_x^2\rangle + \langle v_y^2\rangle)\,,$$

and by using the definitions $v_x = vx'$, $v_y = vy'$ we find

$$E_\mathrm{k} = \frac{1}{2} m\gamma v^2 (\langle x'^2 \rangle + \langle y'^2 \rangle) .$$

As the beam is axi-symmetric, $\langle x'^2 \rangle = \langle y'^2 \rangle$,

$$E_\mathrm{k} = m\gamma v^2 \langle x'^2 \rangle .$$

As the beam is stationary, the equation of motion of a single particle in the beam is $x'' + kx = 0$, and consequently 'depressed optics' is generated, as discussed in Section 6. For this lattice, we find that the modified optics is given by the beta function, $\beta_x = 1/\sqrt{k}$, and $\alpha_x = 0$. For a matched beam, the second-order moments can be related to the depressed optics according to

$$\begin{aligned} \langle x^2 \rangle &= \beta_x \tilde{\varepsilon}_x , \\ \langle x'^2 \rangle &= \gamma_x \tilde{\varepsilon}_x , \\ \langle xx' \rangle &= -\alpha_x \tilde{\varepsilon}_x , \end{aligned} \tag{56}$$

with $\tilde{\varepsilon}_x$ the r.m.s. emittance. In particular, for the constant-focusing case we find $\langle x'^2 \rangle = \frac{1}{\beta_x} \tilde{\varepsilon}_x = \frac{1}{\beta_x^2} \beta_x \tilde{\varepsilon}_x = \frac{1}{\beta_x^2} \langle x^2 \rangle = k \langle x^2 \rangle$. Therefore, the kinetic energy per particle is

$$E_\mathrm{k} = m\gamma v^2 k \langle x^2 \rangle . \tag{57}$$

### 18.2 Potential energy

The transverse potential energy due to the lattice alone is computed by writing the equation of motion in the time domain; in one plane the equation becomes

$$\frac{\mathrm{d}^2}{\mathrm{d}t^2} m\gamma x = m\gamma v^2 k_0 x ,$$

a similar equation is found for the vertical plane with the substitution $x \to y$. Therefore, the potential energy of one particle is then

$$m\gamma v^2 k_0 \left( \frac{x^2}{2} + \frac{y^2}{2} \right) .$$

From this relation, we compute the average potential energy per particle as

$$E_\mathrm{p} = m\gamma v^2 k_0 \langle x^2 \rangle .$$

### 18.3 Field energy

The field energy is the energy necessary to create the beam, i.e., to create the configuration of charges and currents. It consists of two densities of field energy,

$$\frac{\varepsilon_0}{2} \vec{E}^2 , \qquad \frac{1}{2\mu_0} \vec{B}^2 ,$$

the electric and the magnetic field energy. The total field energy is computed by integrating the density of field energy over a volume of length $l$ and extending integration to the beam pipe, of radius $R_\mathrm{p}$. The electric field for a circular Kapchinsky–Vladimirsky coasting beam is given by Eq. (11),

$$E_r(s) = \begin{cases} \frac{\rho(s)}{2\varepsilon_0} r & \text{if} \quad r \le a , \\ \frac{\rho(s) a^2(s)}{2\varepsilon_0} \frac{1}{r} & \text{if} \quad r \ge a . \end{cases} \tag{58}$$

Therefore,

$$\int \frac{\varepsilon_0}{2}\vec{E}^2 \mathrm{d}V = \frac{\rho^2 a^4 \pi l}{4\varepsilon_0}\left[\frac{1}{4} + \ln\left(\frac{R_\mathrm{p}}{a}\right)\right].$$

By using the beam current $I$, we find $I = Av\rho = \pi a^2 v\rho$, which yields

$$\int \frac{\varepsilon_0}{2}\vec{E}^2 \mathrm{d}V = \frac{I^2 l}{4\pi\varepsilon_0 v^2}\left[\frac{1}{4} + \ln\left(\frac{R_\mathrm{p}}{a}\right)\right].$$

The magnetic field $B$ created by a circular 2D Kapchinsky–Vladimirsky beam is given by the Biot–Savart law, namely

$$B_\theta(s) = \begin{cases} \frac{\mu_0 I}{2\pi a^2} r & \text{if} \quad r \le a\,, \\ \frac{\mu_0 I}{2\pi}\frac{1}{r} & \text{if} \quad r \ge a\,. \end{cases} \tag{59}$$

Therefore,

$$\int \frac{1}{2\mu_0}\vec{B}^2 \mathrm{d}V = \frac{\mu_0 I^2 l}{4\pi}\left[\frac{1}{4} + \ln\left(\frac{R_\mathrm{p}}{a}\right)\right].$$

Now using the classical relation $c^2 = 1/(\varepsilon_0\mu_0)$, we find

$$\int \frac{1}{2\mu_0}\vec{B}^2 \mathrm{d}V = \frac{I^2 l}{4\pi\varepsilon_0 c^2}\left[\frac{1}{4} + \ln\left(\frac{R_\mathrm{p}}{a}\right)\right].$$

The total field energy in the volume $V$ is given by the difference of the electric and magnetic energy (see Ref. [3] for more details),

$$E_\mathrm{fV} = \frac{I^2 l}{4\pi\varepsilon_0 c^2}\left[\frac{1}{4} + \ln\left(\frac{R_\mathrm{p}}{a}\right)\right]\left(\frac{1}{\beta^2} - 1\right).$$

Now the number of particles in our integration volume is

$$N_\mathrm{p} = \frac{\rho}{q}\pi a^2 l = \frac{Il}{qv};$$

therefore, the field energy per particle is

$$E_s = qv\frac{I}{4\pi\varepsilon_0 c^2}\left[\frac{1}{4} + \ln\left(\frac{R_\mathrm{p}}{a}\right)\right]\left(\frac{1}{\beta^2} - 1\right). \tag{60}$$

Recalling the definition of perveance, Eq. (19) ,

$$K = \frac{qI}{2\pi\varepsilon_0 m\gamma^3\beta^3 c^3},$$

and replacing $qI$ with the perveance in Eq. (60), we find

$$E_s = Km\gamma\frac{v^2}{8}\left[1 + 4\ln\left(\frac{R_\mathrm{p}}{a}\right)\right].$$

Now using the fact that the beam is stationary, from Eq. (55), we obtain $K = (k_0 - k)a^2$; that is, we find that the field energy per particle is

$$E_s = (k_0 - k)a^2 m\gamma\frac{v^2}{8}\left[1 + 4\ln\left(\frac{R_\mathrm{p}}{a}\right)\right].$$

### 18.4 Total energy, free energy, and emittance growth

The total energy per particle of a stationary beam is the sum of these three types of energy as obtained in the previous three subsections, namely

$$E_n = E_\mathrm{k} + E_\mathrm{p} + E_s$$

which yields

$$E_n = \frac{1}{4} m\gamma v^2 \left\{ ka^2 + k_0 a^2 + (k_0 - k) a^2 \frac{1}{2} \left[ 1 + 4 \ln\left( \frac{R_\mathrm{p}}{a} \right) \right] \right\}, \tag{61}$$

where here we substituted $\langle x^2 \rangle = 4a^2$.

Let us consider a stationary beam characterized by an *initial* envelope $a_i$ and emittance $\mathscr{E}_i$, hence, by an energy per particle $E_{n,i}$. Now let's add to this beam an extra energy per particle $\Delta E_n$: this free energy will make the the beam un-stationary, and the beam envelope will perform oscillations. The principle here invoked is that, due to such additional mechanisms as non-linear or stochastic forces, the free energy $\Delta E_n$ will thermalize. This means that it will spontaneously become 'equally' distributed in all allowed energy forms; hence, the beam will relax into a new *final* stationary state characterized by a new beam size $a_f$, and a new emittance $\mathscr{E}_f$, hence in a new stationary state with energy per particle $E_{nf}$. We therefore find that $E_{nf} = E_{ni} + \Delta E_n$, where $E_{nf}$ is obtained by substituting $k \to k_f, a \to a_f$ into Eq. (61), and $E_{ni}$ is obtained by substituting $k \to k_i, a \to a_i$ into Eq. (61). It is convenient to give the free energy per particle as a function of a dimensionless parameter $h$, as follows

$$\Delta E_n = \frac{1}{2} m\gamma v^2 k_0 a_i^2 h\,. \tag{62}$$

The relation $E_{nf} = E_{ni} + \Delta E_n$ then becomes

$$\frac{a_f^2}{a_i^2} - 1 - \left( 1 - \frac{k_i}{k_0} \right) \ln \frac{a_f}{a_i} = h\,, \tag{63}$$

this relation yields $a_f/a_i$ as a function of $h$. Now we can find the emittance growth from the envelope growth using the straightforward relation

$$\frac{\mathscr{E}_f}{\mathscr{E}_i} = \frac{a_f}{a_i} \left[ 1 + \frac{k_0}{k_i} \left( \frac{a_f^2}{a_i^2} - 1 \right) \right]^{1/2}. \tag{64}$$

Figure 13 shows the emittance growth as a function of the free-energy parameter $h$. There are ten curves for ten different tune depressions: from $Q_x/Q_{0x} = 0.1$, to $Q_x/Q_{0x} = 1$ (i.e., for no space charge). The graph shows that the same free-energy parameter $h$ yields a larger emittance growth, the larger the tune depression.

We now discuss how the free energy is created by mismatching a stationary beam. Consider a matched beam with envelope $a_i$, and now let's mismatch it so that the envelope becomes $a_m$ but preserving the initial beam emittance; let's now call $M = a_m/a_i$ the mismatch factor. Identifying $k_i/k_0 = (Q_{ix}/Q_{0x})^2$, we find that the free-energy parameter $h$ reads

$$h = \frac{1}{2} \left( \frac{Q_{ix}}{Q_{0x}} \right)^2 \left( \frac{1}{M^2} - 1 \right) - \frac{1}{2} \left( 1 - M^2 \right) + \left[ 1 - \left( \frac{Q_{ix}}{Q_{0x}} \right)^2 \right] \ln \left( \frac{1}{M} \right). \tag{65}$$

This relation allows us to compute $h$. We make an example of how to use it. Figure 14 shows a simulation with $Q_{ix}/Q_{0x} = 0.962$, with a beam mismatched by a factor $M = 1.3$. By using Eq. (65), we find the free energy parameter $h = 0.1347$, and the free-energy limit of emittance growth for this value of $h$ is obtained from Eqs. (63) and (64). We find $\mathscr{E}_f/\mathscr{E}_i = 1.145$, which is drawn in Fig. 14 as a dashed green horizontal line. The black and red curves are the horizontal and vertical re-scaled r.m.s. emittances, as obtained from a particle-in-cell simulation. The green curve is the average between them. The simulation shows that the green curve approaches the free-energy limit to a good approximation.

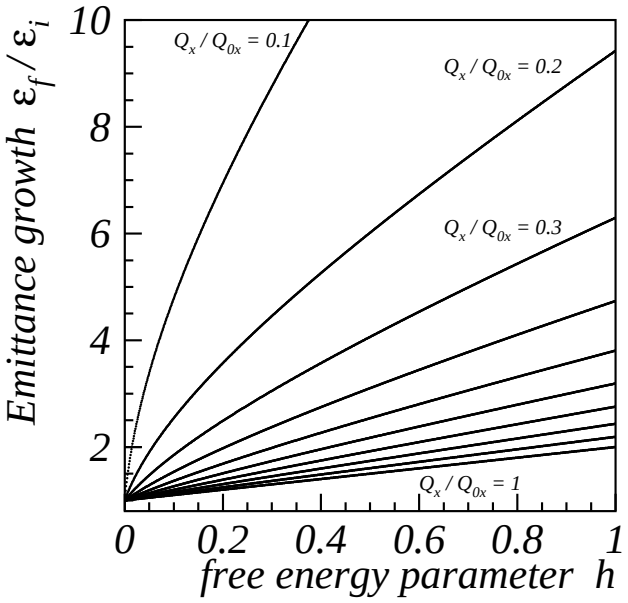


**Fig. 13:** Emittance growth as function of free parameters *h*

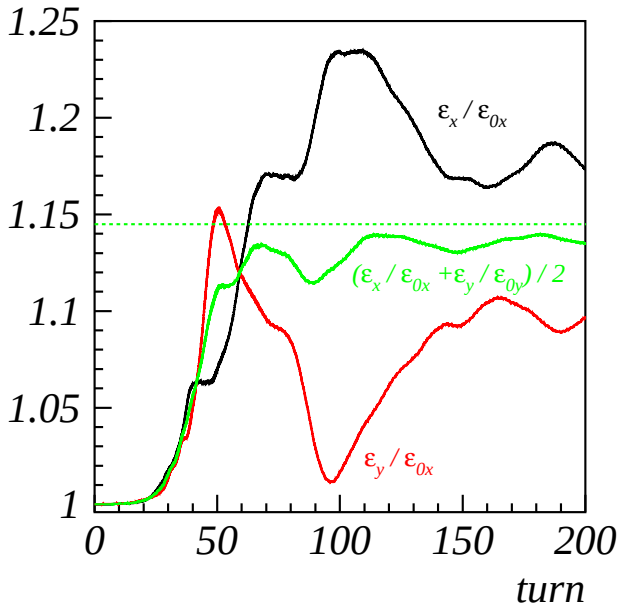


**Fig. 14:** Evolution of beam emittance for mismatched beam in axi-symmetrical constant-focusing lattice. Green: free-energy limit.

## 19 Linear coupling: Chernin equations

In the previous section, we discussed the effect of the free energy on a stationary beam. The mismatch type discussed is obtained by changing the beam size from $a_i$ to $a_m$, and this process creates free energy, which is converted in emittance growth. In doing this, we have addressed only one special type of mismatch, namely the simultaneous mismatch in $x$–$x'$ and $y$–$y'$. However, the mismatch of a beam can be created in much more complex ways by really perturbing the 4D particle distribution. There is, however, one special type of mismatch of relevance when high-intensity beams are considered, and that is the $x$–$y$ mismatch. This is relevant because the space charge forces are directly controlled by the spatial position of the beam distribution.

We observe that in all the previous discussions, we always implicitly assumed the spatial beam profile to be upright. The simplest type of $x$–$y$ mismatch is a rotation in the $x$–$y$ plane of the full beam by an angle $\theta$. The space charge forces respond only to the spatial beam distribution; hence, these forces in the rotated beam will be the same as in the upright distribution, but they will just be rotated as well. The situation is illustrated in Fig. 15.

The left panel shows an upright 2D beam, and the scaled space charge forces as they appear on one particle in the equations of motion are

$$F_x = \frac{2K}{a(a+b)}X, \qquad F_y = \frac{2K}{b(a+b)}Y, \tag{66}$$

where $X,Y$ are the co-ordinates of the test particle in the reference frame where the beam is upright. The right panel of Fig. 15 shows the beam tilted. The axes and forces of the original reference frame, where the beam is upright, are depicted in black. The axis of the new reference frame is depicted in blue. The test particle now has new co-ordinates $x,y$, and the forces acting on the particle are the projection of the scaled space charge force vector (red) along the $x$ and $y$ axes (blue). It is therefore possible to find the $X,Y$ co-ordinates in the upright reference frame from the particle co-ordinates $x,y$ in the frame of the tilted beam, and there the space charge forces are given by Eq. (66). At that point, we decompose $F_x,F_y$ along the new axes, and find the new components of the scaled space charge force $f_x,f_y$ along the axis $x,y$. By applying this procedure mathematically, we obtain the following scaled forces:

$$\begin{aligned} f_x &= \left[\frac{2K}{a(a+b)}\cos^2\theta + \frac{2K}{b(a+b)}\sin^2\theta\right]x + \sin\theta\cos\theta\left[\frac{2K}{a(a+b)} - \frac{2K}{b(a+b)}\right]y, \\ f_y &= \left[\frac{2K}{b(a+b)}\cos^2\theta + \frac{2K}{a(a+b)}\sin^2\theta\right]y + \sin\theta\cos\theta\left[\frac{2K}{a(a+b)} - \frac{2K}{b(a+b)}\right]x. \end{aligned} \tag{67}$$

We observe immediately that the tilting of the beam produces a coupling between the horizontal and vertical planes. It is interesting that the coefficient of the coupling terms in $f_x,f_y$ is the same. This appears exactly as if there would be a skew quadrupole acting on the test particle.

The situation is now more complex than that discussed in Section 9. In fact, the former equation of motion of a single particle, Eq. (34), now takes a more complex form, namely

$$\frac{\mathrm{d}^2x}{\mathrm{d}s^2} + k_{0x}(s)x - \frac{2K}{a+b}\left(\frac{1}{a}\cos^2\theta + \frac{1}{b}\sin^2\theta\right)x - \sin\theta\cos\theta\frac{2K}{a+b}\left(\frac{1}{a} - \frac{1}{b}\right)y = 0\,. \tag{68}$$

A similar equation can be derived for the motion in the $y$ plane. The coupling term has an important consequence if we try to compute the r.m.s. envelope equation. In fact, in Eq. (32), the second-order moment $\langle xx''\rangle$ will now produce one additional term proportional to the second-order moment $\langle xy\rangle$. Note that the second-order moment $\langle xy\rangle$, is directly proportional to $\sin(2\theta)$. This simply means that the evolution of $\tilde{x}$ depends on coupled second-order moments, and it is therefore not possible to write two separate equations of motion for horizontal and vertical planes.

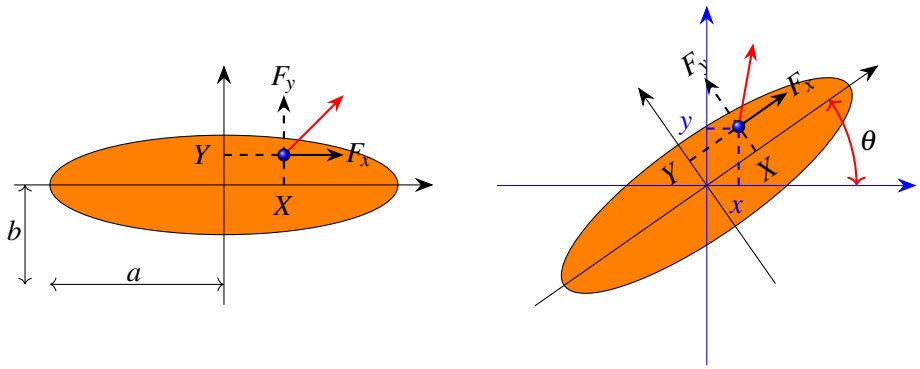


**Fig. 15:** Decomposition of forces in tilted beam. Left-hand side: upright beam and test particle in it, with space charge forces. Right-hand side: the same beam, now tilted by $\theta$. The space charge force is now decomposed along new axes.

The problem has to be discussed in full generality by describing the evolution of all second-order moments, which forms the $4\times 4$ matrix

$$\Sigma_{i,j} = \langle v_i v_j \rangle - \langle v_i \rangle \langle v_j \rangle ,$$

where $\vec{v} = (x, x', y, y')$. The evolution of $\Sigma$ is derived by Chernin [8] as

$$\Sigma' = M\Sigma + (M\Sigma)^{\mathrm{T}}, \tag{69}$$

where the symbol $^{\mathrm{T}}$ refers to the operation to transpose a matrix. The matrix $M$ has the form

$$M = \begin{pmatrix} 0 & 1 & 0 & 0 \\ -\tilde{k}_x & 0 & \tilde{j} & 0 \\ 0 & 0 & 0 & 1 \\ \tilde{j} & 0 & -\tilde{k}_y & 0 \end{pmatrix} , \tag{70}$$

where

$$\tilde{k}_x = k_{0x} - q_{xx} , \qquad \tilde{k}_y = k_{0y} - q_{yy} , \qquad \tilde{j} = j_0 + q_{xy} , \tag{71}$$

and

$$q_{xx} = \frac{K}{2}\frac{S_y}{S_0(S_x+S_y)} , \qquad q_{yy} = \frac{K}{2}\frac{S_x}{S_0(S_x+S_y)} , \qquad q_{xy} = -\frac{K}{2}\frac{\Sigma_{13}}{S_0(S_x+S_y)} , \tag{72}$$

and

$$S_x = \Sigma_{11} + S_0 , \quad S_y = \Sigma_{33} + S_0 , \quad S_0 = \sqrt{\Sigma_{11}\Sigma_{33} - \Sigma_{13}^2} .$$

The quantities $k_{0x}, k_{0y}$ are the usual focusing strength, $j_0$ is the skew strength produced by skew quadrupoles. The terms $q_{xx}, q_{yy}$ are the space charge defocusing effect in the $x$ and $y$ planes, and their form resembles Eq. (66). When $\Sigma_{13} = 0$, then $q_{xx}$, and $q_{yy}$ become exactly equal to Eq. (66). The term $q_{xy}$ is a self-coupling created by the space charge. It is now possible that the tilted beam produces a self-linear coupling that affects the beam evolution in the $x$–$y$ plane. This coupling derives from the last term in Eq. (68).

Figure 16 shows the evolution of the beam emittances in a lattice with a skew quadrupole calculated using Eq. (69). The simulation is performed in proximity to the linear coupling resonance

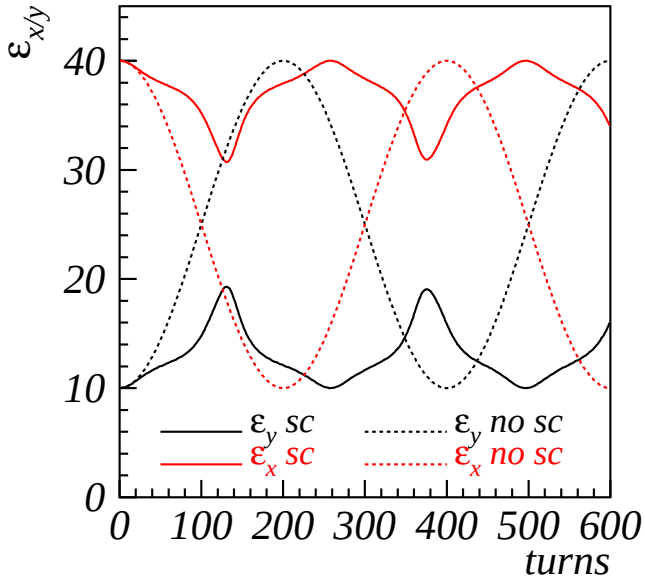


**Fig. 16:** Beam emittance evolution for low-intensity beam (dashed curves), and high-intensity beam (solid curves)

$Q_{0x} - Q_{0y} = N$ (see also Ref. [9] for further details). The graph shows a simulation of a beam with initial Kapchinsky–Vladimirsky emittances of $\varepsilon_x = 40$ mm-mrad and $\varepsilon_y = 10$ mm-mrad. The dashed curve shows the case without space charge when the tunes sit on the linear coupling resonance. The skew quadrupole exciting the resonance produces an emittance exchange in 200 machine turns. The solid curves show the emittance evolution as computed with Chernin equations when the high intensity yields $\Delta Q_y = -0.2$. The tunes are $Q_{0y} = 3.2$ and $Q_{0x} \simeq 4.16$. It can be seen that the space charge prevents the full emittance exchange. However, the sum of the two emittance is preserved.

## 20 The Montague resonance

The possibility of a beam affecting itself via space charge is quite a relevant topic. In the previous section we discussed the linear coupling, which in Eq. (68) is shown by an extra coupling term in $y$, the strength of which depends on the tilting of the beam.

However, more complex effects may be created by space charge. In particular, the space charge may influence particle motion even for an upright beam. In fact, for a 2D Gaussian upright beam, the scaled force on a beam particle is

$$\begin{aligned} F_x(x,y) &= K\left[\frac{1}{a(a+b)}x - \frac{2a+b}{6a^3(a+b)^2}x^3 - \frac{1}{2ab(a+b)^2}xy^2 + \ldots\right], \\ F_y(x,y) &= K\left[\frac{1}{b(a+b)}y - \frac{2b+a}{6b^3(a+b)^2}y^3 - \frac{1}{2ba(a+b)^2}yx^2 + \ldots\right], \end{aligned} \tag{73}$$

where $a, b$ are the r.m.s. sizes of the distribution with

$$n(x,y,s) = \frac{1}{2\pi ab}\exp\left[-\frac{1}{2}\left(\frac{x^2}{a^2} + \frac{y^2}{b^2}\right)\right].$$

For a frozen beam, the forces in Eq. (73) are of incoherent type, and act on a single particle as if they are given by an external element. The main difference between the scaled forces in Eq. (73), and those in Eq. (67) is that for an upright beam $\theta = 0$; hence, the coupling strength in Eq. (67) disappears, while

in Eq. (73) a coupling term with strength

$$-\frac{K}{2ba(a+b)^2}$$

remain unaffected. The consequences of this coupling term go beyond the linear motion as the forces that it generates are non-linear.

According to the theory of the resonances [10, 11], the excitation of a resonance depends on the strength of the harmonics of the driving term, which can be expressed from the potential of the forces. In particular the potential of the coupling term in Eq. (73) reads

$$\frac{K}{4ba(a+b)^2}y^2x^2\,.$$

This term excites the resonances $2Q_x \pm 2Q_y = N$. Of particular interest is the resonance $2Q_x - 2Q_x = 0$, which is quite unusual in single-particle dynamics, as the zero-order harmonics are very weak because non-linear components are typically localized in distinct spots around the machine. The strength of the zero-order harmonics is proportional to the integral

$$K\int_0^L \frac{\beta_{0x}(s)\beta_{0y}(s)}{a(s)b(s)[a(s)+b(s)]^2}\exp\left\{i2\left[\phi_x(s)-2\pi Q_{0x}\frac{s}{L}\right]-i2\left[\phi_y(s)-2\pi Q_{0y}\frac{s}{L}\right]\right\}\mathrm{d}s\,,$$

where it is evident that the driving term is proportional to the perveance. In the formula are used the phase advances defined as $\phi_x(s) = \int_0^s ds/\beta_{0x}(s), \phi_y(s) = \int_0^s ds/\beta_{0y}(s)$. This coupling resonance is found in any ring near the diagonal $Q_x = Q_y$, but it is driven by the fourth-order term in the space charge potential. The first study of this space charge resonance was made by Montague [12]. A simple demonstration of the effect of this resonance is obtained by integrating the dynamics of the following simplified system

$$\begin{aligned} x'' + \left(\frac{Q_{0x}}{R}\right)^2 x &= F_x(x,y)\,,\\ y'' + \left(\frac{Q_{0y}}{R}\right)^2 y &= F_y(x,y)\,, \end{aligned} \tag{74}$$

with $F_x, F_y$ given by Eq. (73). These equations describe the dynamics of particles under the effect of the second- and fourth-order terms of the frozen potential. The left panel of Fig. 17 shows the beam response as a function of the working point of a Gaussian beam with r.m.s. emittances of $\tilde{\varepsilon}_x = 40$ mm-mrad and $\tilde{\varepsilon}_y = 20$ mm-mrad. The red curve shows the average r.m.s. emittances $\tilde{\varepsilon}_y$, and the black curve shows the average r.m.s. emittances $\tilde{\varepsilon}_x$. These averages are computed with all the r.m.s. beam emittance from turn 250 to turn 1000. The strength of the perveance $K$ produces a tune-shift of $\Delta Q_{0x} = -0.05$ in the Gaussian beam. The fourth-order coupling term in the potential creates a dynamics which brings the two emittances closer so that the depressed tunes are closer to the resonance $2Q_x - 2Q_y = 0$.

In this first discussion, which follows the tracks of Montague, the space charge force is frozen (i.e., $a_0(s), b_0(s)$ of Eq. (10) follow the machine optics as $a_0(s) = \sqrt{\beta_{0x}(s)\mathscr{E}_x}$ and $b_0(s) = \sqrt{\beta_{0y}(s)\mathscr{E}_y}$ if the intensity is low, otherwise follow the depressed optics as discussed in Section 6).

The results of the left panel of Fig. 17 are obtained by including only the first two terms of the space charge potential; when all the terms of the frozen potential are included, the picture changes, as shown in the right panel of Fig. 17. Here, we see that the emittances are exchanged more, and the stop-band becomes narrower. Surely, this modification stems from the inclusion of all resonant terms and all non-resonant terms in the dynamics, to produce a more realistic detuning.

We observe that in Fig. 17 the r.m.s. emittances of the test particles exchange by a significant amount, owing to the effect of the resonance; consequently, we expect that the beam sizes $a, b$ will also change accordingly. However, in Fig. 17 this effect is removed as we have kept the sizes $a, b$ in

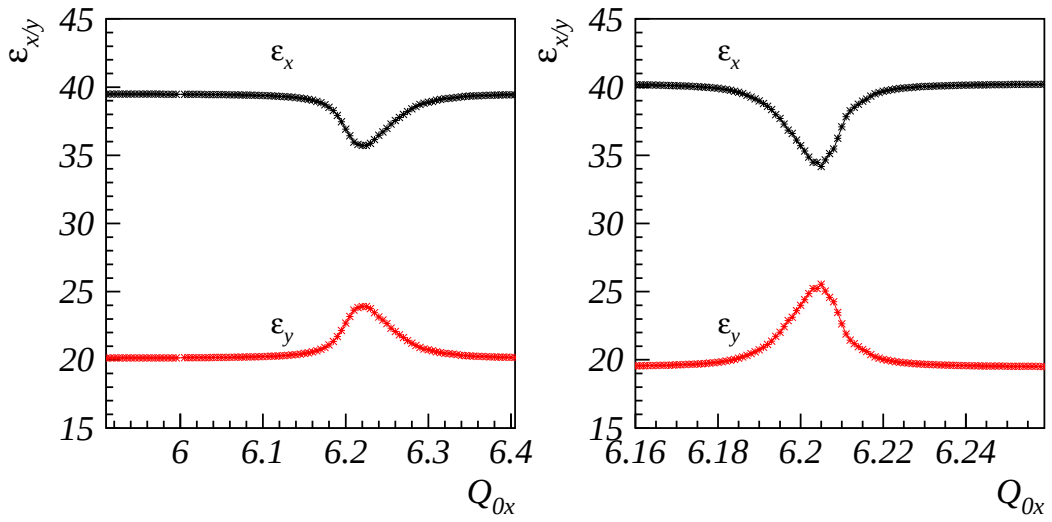


**Fig. 17:** Average $\tilde{\varepsilon}_x, \tilde{\varepsilon}_y$ in 750 turns after beam. Left-hand side: space charge computed using the second- and third-order potentials. Right-hand side: all terms of the potential are included in the calculation.

the simulations frozen to the optics. If we let the beam size $a, b$ vary with time, the change of beam size will feed back to the space charge; consequently, the dynamics will not produce the results of the right panel of Fig. 17, as the variation of $a, b$ will be included in the beam evolution. This effect of self-consistency will affect the degree of emittance exchange, as shown in Fig. 18. The vertical tune is set to $Q_{0y} = 6.21$, and the incoherent tune-shift is $\Delta Q_y = -0.05$. A detailed discussion of these studies is reported in Ref. [13]. The complexity of the Montague resonance, however, exceeds the analysis so far presented, as the condition of the Montague resonance is also the condition of the instability of the beam collective modes, introduced in Sections 14 and 15. In fact, it can be shown, by a perturbative Vlasov analysis of the collective modes, that some of them become unstable under certain conditions. Figure 19 shows an example of the dependence of the growth rates on $Q_{0x}$ for the fourth-order collective modes in a coasting beam with a transverse Kapchinsky–Vladimirsky distribution (from Ref. [13]). These modes are excited and contribute to the dynamics of the Montague resonance, which becomes a mix of incoherent and coherent effects. The dominance of the coherent effects is found for distributions closer to a Kapchinsky–Vladimirsky distribution, where the dynamics of the emittance exchange is driven by the growth of the collective modes rather than the fourth-order potential à la Montague. For a Gaussian distribution, the collective modes are instead damped by the non-linear field, but the very same field acts according to the original study of Montague and triggers an emittance exchange anyway. Experimental and simulation benchmarking studies are found in Ref. [14].

## 21 Space charge as incoherent force

If we look again at Eq. (73), the expansion shows the existence of non-coupled terms. Therefore, the third-order components of the force can excite fourth-order resonances if the corresponding driving term is excited by the lattice structure. This is shown in Fig. 20, where a multiparticle particle-in-cell simulation shows that space charge creates the characteristic four islands of a fourth-order resonance. In this example, the horizontal tune is set above the fourth-order resonance, which is excited by a lattice composed of a number of FODO cells equal to the harmonics of the resonance: specifically, here we used a lattice formed with 25 identical FODO cells; the tunes are $Q_{0x} = 6.26$, $Q_{0y} = 6.73$, and the beam is Gaussian with r.m.s. emittances $\tilde{\varepsilon}_x = 40$ mm-mrad, $\tilde{\varepsilon}_y = 20$ mm-mrad. The space charge incoherent

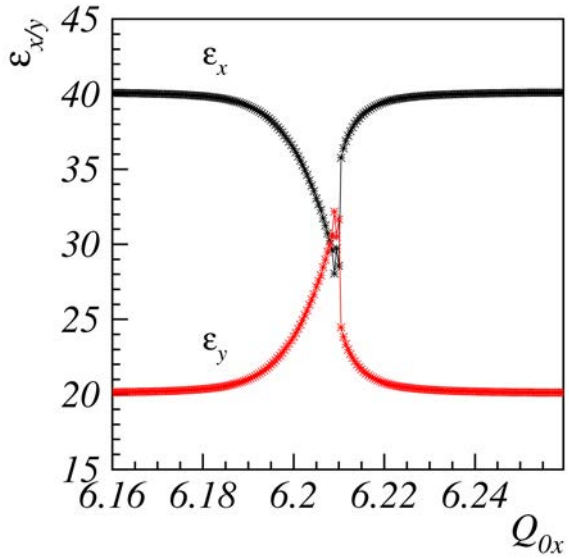


**Fig. 18:** Emittance exchange obtained via fully self-consistent simulation. It is clear that the symmetry in the exchange is broken by the change of beam sizes.

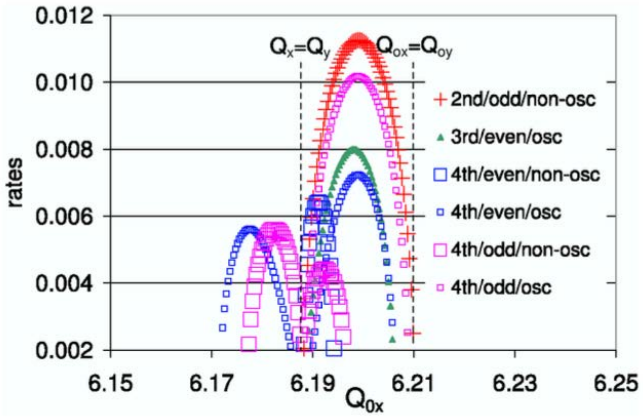


**Fig. 19:** Example of growth rate of the fourth-order collective modes in a Kapchinsky–Vladimirsky distribution (from Ref. [13]). The stop-band of the modes coincides with the Montague stop-band found in the self-consistent simulations.

tune-shifts are $\Delta Q_{0x} \simeq -0.05$ and $\Delta Q_{0y} \simeq -0.065$. These are relatively modest, but the effect is still remarkable. The original work on the excitation of fourth-order resonances by space charge is found in Ref. [15]. More generally, the non-linear space charge force will exhibit all the odd-order non-linear components. Each of these components can excite a structure resonance if the harmonic number of a non-linear force component satisfies the resonance condition for that non-linear term. A spectral analysis of the $x$–$y$ components of the space charge force will reveal which harmonics are strongly excited.

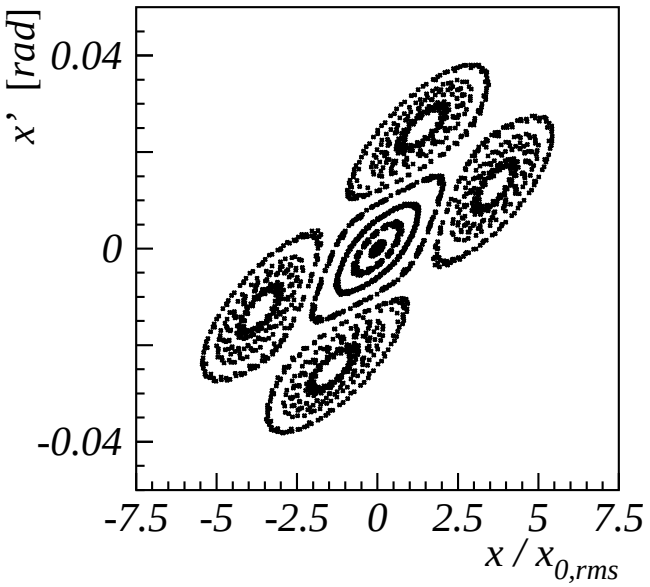


**Fig. 20:** Poincaré map of a few test particles in a full beam tracked with a particle-in-cell code through a lattice formed by FODO cells. The four islands clearly show that the forth-order resonance is excited. The $x$ axis is plotted in 'normalized' co-ordinates to highlight that the four islands are located, in this example, beyond the tails of the beam distribution.

## 22 The longitudinal envelope equation

The discussion made for the transverse effects of space charge can be repeated for the longitudinal plane. We recall that the equation of motion in a linearized RF bucket is

$$z'' + k_{0z} z = 0\,, \tag{75}$$

with

$$k_{0z} = \frac{qV\eta h}{2\pi R^2 mc^2 \gamma_0 \beta_0^2}$$

the longitudinal focusing [3]. The derivative has the usual meaning $()' = \mathrm{d}()/\mathrm{d}s$. Here, $q$ is the charge state; $V$ is the maximum voltage applied to the cavity; $\eta = \alpha - 1/\gamma_0^2$ is the slip factor and $\alpha$ the momentum compaction; $h$ is the harmonic number of the cavity, for which the angular frequency is $\omega_{\mathrm{rf}} = 2\pi h/\tau_0$, with $\tau_0$ the revolution time, $R$ the average accelerator radius, and $m$ the particle mass. The stability of the longitudinal oscillations requires $k_{0z} > 0$; hence, $V$ must be selected according to the sign of the slip factor $\eta$.

In this notation, we can describe the particle dynamics in terms of the co-ordinates $(z, z')$, as we did for the transverse plane. The relation of $z'$ with the off momentum of a particle is $z' = -\eta\,\delta p/p$. In analogy with the discussion made for the transverse dynamics, we now consider a matched distribution with the longitudinal optics created by Eq. (75), for a small intensity. Any function

$$\rho_{zz'}(z,z') = Qn(z,z') = Q\frac{1}{\pi \mathscr{E}_z}\tilde{n}\left(\frac{\varepsilon_{0z}(z,z')}{\mathscr{E}_z}\right)$$

represents a matched distribution in the longitudinal plane. $Q$ is the total charge in the bunch, and $\mathscr{E}_z$ is a 'scaling' factor that defines the geometrical extension of the distribution in the phase space. $n(z,z')$ is

the normalized distribution function. The normalization condition requires that the function $\tilde{n}(t)$ satisfies $\int_0^\infty \tilde{n}(t)\mathrm{d}t = 1$. In analogy with the transverse plane discussion,

$$\varepsilon_{0z}(z,z') = \varepsilon_{0z} = \sqrt{k_{0z}}z^2 + \frac{1}{\sqrt{k_{0z}}}z'^2 \tag{76}$$

is the single-particle emittance. If we identify $\beta_{0z} = 1/\sqrt{k_{0z}}$, Eq. (76) is the Courant–Snyder invariant for a constant-focusing channel. Following the approach used in the transverse plane, we may now consider several types of function. Of particular interest is the distribution

$$n(z,z') = \frac{1}{\pi\mathscr{E}_z}\frac{3}{2}\sqrt{1-\frac{\varepsilon_{0z}}{\mathscr{E}_z}}\,.$$

The sizes of this distribution are $z_m = \sqrt{\beta_{0z}\mathscr{E}_z}$, $z'_m = \sqrt{1/\beta_{0z}\mathscr{E}_z}$ and the longitudinal charge-line density, i.e., the projection of $\rho_{zz'}$ to $z$ axis becomes

$$\rho_L(z) = \int_{-z'_m\sqrt{1-z^2/z_m^2}}^{z'_m\sqrt{1-z^2/z_m^2}} Qn(z,z')\mathrm{d}z' = Q\frac{3}{4z_m}\left(1-\frac{z^2}{z_m^2}\right). \tag{77}$$

As expected, the particle distribution will create a longitudinal electric field. Unlike the derivation from the transverse plane, the longitudinal space charge electric field in the laboratory frame is computed as

$$E_z = -\frac{g}{4\pi\varepsilon_0\gamma_0^2}\frac{\partial\rho_L(z)}{\partial z}\,, \tag{78}$$

see Ref. [3] for a derivation. The factor $g$ is a geometric factor; it incorporates the effect of the image charge on the longitudinal electric field. For long bunches, $g \simeq 0.67 + 2\ln(r_{\mathrm{pipe}}/a)$, with $a$ the transverse beam size [3].

If we include the longitudinal space charge electric field in the equation of motion, we obtain

$$z'' + k_{0z}z = -\frac{\eta q}{mc^2\beta_0^2\gamma_0}E_z\,,$$

and for the particular electric field of Eq. (78) we find

$$z'' + k_{0z}z = \frac{Zr_{\mathrm{p}}g\eta}{eA\beta_0^2\gamma_0^3}\frac{\partial\rho_L(z)}{\partial z}\,.$$

where $q = Ze$, $m = Am_{\mathrm{p}}$, with $e$ the electron charge, and $m_{\mathrm{p}}$ the proton mass; $r_{\mathrm{p}} = 1/(4\pi\varepsilon_0)e^2/(m_{\mathrm{p}}c^2)$ is the classical radius of the proton. Now we consider the frozen parabolic longitudinal charge-line density described by Eq. (77), and the equation of motion becomes

$$z'' + k_{0z}z = -\frac{3}{2}\frac{NZ^2r_{\mathrm{p}}g\eta}{A\beta_0^2\gamma_0^3}\frac{z}{z_m^3}\,. \tag{79}$$

In analogy with the discussion in the transverse plane, we define a longitudinal perveance $K_{\mathrm{L}}$ as

$$K_{\mathrm{L}} = -\frac{3}{2}\frac{NZ^2r_{\mathrm{p}}g\eta}{A\beta_0^2\gamma_0^3}\,,$$

and the equation of motion takes the following form

$$z'' + k_{0z}z - K_{\mathrm{L}}\frac{z}{z_m^3} = 0\,. \tag{80}$$

This equation is the equivalent of Eqs. (20) and (21) for the transverse plane.

We now can define an r.m.s. envelope as $\tilde{z} = \sqrt{\langle z^2 \rangle}$, and through straightforward algebra we find

$$\tilde{z}'' + k_{0z}\tilde{z} - K_{\mathrm{L}}\frac{\tilde{z}}{z_m^3} - \frac{\varepsilon_{zz'}^2}{\tilde{z}^3} = 0\,,$$

where we define the r.m.s. longitudinal emittance as

$$\tilde{\varepsilon}_{zz'}^2 = \langle z^2 \rangle \langle z'^2 \rangle - \langle z z' \rangle^2\,.$$

For the parabolic distribution, we find that the relations between the r.m.s. sizes and the edge of the particle distribution are

$$z_m = \sqrt{5}\sqrt{\langle z^2 \rangle}, \quad z'_m = \sqrt{5}\sqrt{\langle z'^2 \rangle}\,,$$

from which we can compute the emittance of the full distribution as $\varepsilon_{\mathrm{L}}^2 = z_m^2 (z'_m)^2$, and hence $\tilde{\varepsilon}_{zz'}^2 = \langle z^2 \rangle \langle z'^2 \rangle = \varepsilon_{\mathrm{L}}^2/25$. The complete longitudinal envelope equation reads

$$z_m'' + k_{0z} z_m - K_{\mathrm{L}}\frac{1}{z_m^2} - \frac{\varepsilon_{\mathrm{L}}^2}{z_m^3} = 0\,.$$

### 22.1 Effect of space charge and self-consistency

We observe that the electric field generated by the parabolic distribution is linear. Therefore in Eq. (80), a depressed longitudinal focusing strength is well defined as

$$k_z = k_{0z} - \frac{K_{\mathrm{L}}}{z_m^3}\,.$$

Therefore, we can again define a beam matched with the space charge, and define

$$\rho_{zz'}(z,z') = Q\frac{1}{\pi \mathscr{E}_z}\tilde{n}\left(\frac{\varepsilon_z(z,z')}{\mathscr{E}_z}\right)\,,$$

where now

$$\varepsilon_z(z,z') = \varepsilon_z = \sqrt{k_z} z^2 + \frac{1}{\sqrt{k_z}} z'^2\,.$$

This longitudinal particle distribution creates linear space charge forces. Linear forces are consistent with Courant–Snyder invariants, which means that the type of longitudinal particle distribution will remain unchanged. This is equivalent to what happened in the transverse Kapchinsky–Vladimirsky distribution.

The direct proof that the parabolic distribution satisfies the stationary Vlasov equation, hence that the distribution type does not change, was made by Neuffer [16].

We conclude with the observation that the results reported here are very general and apply even if the particle distribution is not upright. The parabolic distribution will still generate a linear electric field, although the longitudinal 'ellipses' are no longer upright. See an example in Ref. [17].

## 23 Conclusion

This paper is meant to provide a quick overview of space charge effects. This field is more broad than what is here presented. Topics presented are complementary to other CERN Accelerator School proceedings, for example Ref. [18] for further discussions on beam transport in presence of space charge. The topic of tune-shift from self-field and image charge, not covered here, is treated in Ref. [19]. Other derivations, also including a discussion of the space charge limit are found in Ref. [20]. More recent topics, such as the interplay of space charge and machine resonances, are omitted, as are topics of current research.

## Acknowledgements

I thank Frederik Kesting, Yuan Yaoshuo, and Ingo Hofmann for reading and commenting on this paper.

## References

[1] E.D. Courant and H.S. Snyder, *Ann. Phys. (N.Y.)* **3** (1958) 1. https://doi.org/10.1016/0003-4916(58)90012-5

[2] O.D. Kellog, *Foundation of Potential Theory* (Dover Publications, New York, 1953).

[3] M. Reiser, *Theory and Design of Charged Particle Beams* (Wiley-VCH, Weinheim, 2004).

[4] F.J. Sacherer, *IEEE Trans. Nucl. Sci.* **18** (1971) 1015. https://doi.org/10.1109/TNS.1971.4326265

[5] I. Hofmann, *Phys. Rev. E* **57** (1998) 4713. https://doi.org/10.1103/PhysRevE.57.4713

[6] R. Bartolini *et al.*, *Part. Accel.* **52** (1996) 147.

[7] K.Y. Ng, *Physics of Intensity Dependent Beam Instabilities* (World Scientific, Singapore, 2006).

[8] D. Chernin, *Part. Accel.* **24** (1988) 29.

[9] G. Franchetti *et al.*, *Phys. Rev. Lett.* **94** (2005) 194801. https://doi.org/10.1103/PhysRevLett.94.194801

[10] G. Guignard, A general treatment of resonances in accelerators, CERN-1978-011 (CERN, Geneva, 1978), http:/dx.doi.org/10.5170/CERN-1978-011.

[11] A. Schoch, Theory of linear and non-linear perturbations of betatron oscillations in alternating gradient synchotrons, CERN-1957-021 (CERN, Geneva, 1957), http://dx.doi.org/10.5170/CERN-1957-021.

[12] B.W. Montague, Fourth-order coupling resonance excited by space-charge forces in a synchrotron, CERN-1968-038 (CERN, Geneva, 1968), http://dx.doi.org/CERN-1968-038.

[13] I. Hofmann and G. Franchetti, *Phys. Rev. Spec. Top. Accel. Beams* **9** (2006) 054202. https://doi.org/10.1103/PhysRevSTAB.9.054202

[14] J. Qiang *et al.*, Numerical simulation study of the montague resonance at the CERN proton synchrotron, 3rd Int. Particle Accelerator Conf., New Orleans, 2012, p. WEPPR011.

[15] S. Machida, *Nucl. Instrum. Methods A* **A309** (1991) 43. https://doi.org/10.1016/0168-9002(91)90091-4

[16] D. Neuffer, *IEEE Trans. Nucl. Sci.* **26** (1979) 3031. https://doi.org/10.1109/TNS.1979.4329929

[17] G. Franchetti *et al.*, *Phys. Rev. Spec. Top. Accel. Beams* **3** (2000) 084201. https://doi.org/10.1103/PhysRevSTAB.3.084201

[18] I. Hofmann, in Proceedings of the CAS-CERN Accelerator School: 5th Advanced Accelerator Physics Course, Rhodes, Greece, 20 September-1 October 1993, edited by S. Turner, CERN-1995-006 (CERN, Geneva, 1995), pp. 941–954, http://dx.doi.org/10.5170/CERN-1995-006.941.

[19] A. Hoffmann, in Proceedings of the CAS-CERN Accelerator School: 5th General Accelerator Physics Course, Jyvaskyla, Finland, 7-18 September 1992, CERN-1994-001 (CERN, Geneva, 1994), pp. 329–348, http://dx.doi.org/10.5170/CERN-1994-001.329.

[20] K. Schindl, in Proceedings of the CAS-CERN Accelerator School on Accelerator Physics, Zeuthen, Germany, 15-16 September 2003, CERN-2006-002 (CERN, Geneva, 2006), pp. 305–320, http://dx.doi.org/10.5170/CERN-2006-002.305.